Article

Cell

Cryo-EM Structure of Human Dicer and Its Complexes with a Pre-miRNA Substrate

Graphical Abstract

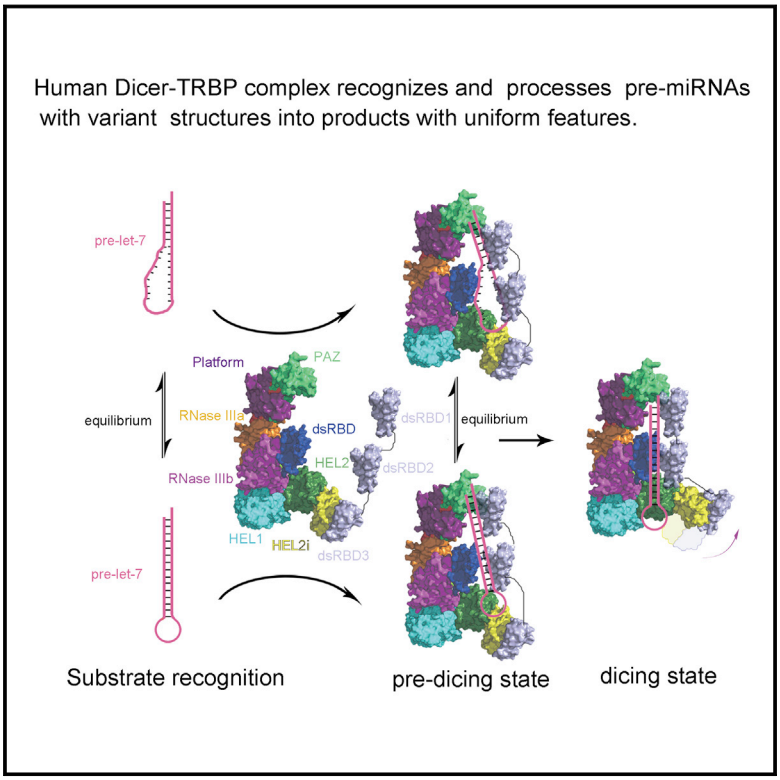

Authors

Zhongmin Liu, Jia Wang, Hang Cheng, Xin Ke, Lei Sun, Qiangfeng Cliff Zhang, Hong-Wei Wang

Correspondence

hongweiwang@tsinghua.edu.cn

In Brief

Structural analysis of human Dicer shows how it collaborates with an accessory protein to position a pre-miRNA substrate for processing.

Highlights

- Cryo-EM structure of apo-hDicer-TRBP complex at 4.4 Å
- Cryo-EM structures of hDicer-TRBP in complex with pre-let-7 RNA
- Two conformers of pre-let-7 bound by the hDicer-TRBP complex in a pre-dicing state
- Human Dicer-TRBP complex could stabilize the stem of pre-miRNA

Data resources

5ZAK
5ZAL
5ZAM
GSE110516

Liu et al., 2018, Cell *173*, 1191–1203
May 17, 2018
https://doi.org/10.1016/j.cell.2018.03.080

CellPress

Article

Cell

Cryo-EM Structure of Human Dicer and Its Complexes with a Pre-miRNA Substrate

Zhongmin Liu,[1,3,4] Jia Wang,[1,3,4] Hang Cheng,[1,2,3] Xin Ke,[1,3] Lei Sun,[1] Qiangfeng Cliff Zhang,[1] and Hong-Wei Wang[1,5,*]
[1]Ministry of Education Key Laboratory of Protein Sciences, Tsinghua-Peking Joint Center for Life Sciences, Beijing Advanced Innovation Center for Structural Biology, School of Life Sciences, Tsinghua University, Beijing, China 100084
[2]Joint Graduate Program of Peking-Tsinghua-NIBS, School of Life Sciences, Tsinghua University, Beijing, China 100084
[3]These authors contributed equally
[4]Senior author
[5]Lead Contact
*Correspondence: hongweiwang@tsinghua.edu.cn
https://doi.org/10.1016/j.cell.2018.03.080

SUMMARY

Human Dicer (hDicer) is a multi-domain protein belonging to the RNase III family. It plays pivotal roles in small RNA biogenesis during the RNA interference (RNAi) pathway by processing a diverse range of double-stranded RNA (dsRNA) precursors to generate ~22 nt microRNA (miRNA) or small interfering RNA (siRNA) products for sequence-directed gene silencing. In this work, we solved the cryo-electron microscopy (cryo-EM) structure of hDicer in complex with its cofactor protein TRBP and revealed the precise spatial arrangement of hDicer's multiple domains. We further solved structures of the hDicer-TRBP complex bound with pre-let-7 RNA in two distinct conformations. In combination with biochemical analysis, these structures reveal a property of the hDicer-TRBP complex to promote the stability of pre-miRNA's stem duplex in a pre-dicing state. These results provide insights into the mechanism of RNA processing by hDicer and illustrate the regulatory role of hDicer's N-terminal helicase domain.

INTRODUCTION

Small RNAs, including micro RNA (miRNAs), small interfering RNAs (siRNAs), and Piwi-interacting RNAs (piRNAs), are central players in RNAi pathways. These molecules recognize their gene targets by sequence matching and induce gene silencing via effector proteins such as the Argonaut-family proteins (Filipowicz et al., 2008; Ha and Kim, 2014; Kim et al., 2009). The latest miRNA database (miRBase) indicates that there are more than 2,600 identified miRNAs that regulate most of the protein-coding genes in human, indicating a significant role of small RNAs in many cellular processes (Friedman et al., 2009; Ha and Kim, 2014; Kozomara and Griffiths-Jones, 2014). Small RNA biogenesis normally involves steps in which specific endoribonucleases, such as Drosha and Dicer, consecutively cleave long RNA precursors with double-stranded features into final short double-stranded RNAs (dsRNAs) (Han et al., 2004; Kim et al., 2009; Lee et al., 2002, 2003). In humans, a single-copy hDicer is responsible for the last cleavage step, which processes a diverse range of precursors into duplex products that have a common feature of a 5′ phosphate, 2 nt 3′ overhang and a length of approximately 22 bp (Ambros et al., 2003). The duplex products are finally loaded into Argonaut proteins to form silencing complexes (Bernstein et al., 2001; Betancur and Tomari, 2012; Kim et al., 2014, 2016). The small RNA biogenesis, especially the Drosha and Dicer processing, is highly regulated by cofactor proteins, RNA precursors, and post-transcriptional modifications (Castilla-Llorente et al., 2013; Heale et al., 2009; Heo et al., 2012; Lee and Doudna, 2012; Lee et al., 2006; Starega-Roslan et al., 2011). The mechanism and regulation of these processes, however, remain enigmatic.

As a member of the endoribonuclease III family, the 218 kDa hDicer protein harbors two RNase III domains (RNase IIIa and RNase IIIb) and a dsRNA-binding domain (dsRBD) in its C-terminal region, all of which are conserved in other RNase III proteins including Dicers in other eukaryotic species, eukaryotic Droshas, and the bacterial RNase IIIs (Bernstein et al., 2001; Blaszczyk et al., 2004; Court et al., 2013; Nicholson, 2014). Different from other RNase III proteins, hDicer has an N-terminal DExD/H-box helicase domain, a DUF283 domain, a Platform domain, and a PAZ domain (Figure 1A) (Bernstein et al., 2001). The DExD/H-box helicase domain has been shown to bind certain hDicer-associated proteins and the terminal loop of pre-miRNAs (Daniels et al., 2009; Du et al., 2008; Lee et al., 2006; Ota et al., 2013; Tsutsumi et al., 2011). The DUF283 domain is expected to have a similar fold to dsRBD based on computational prediction (Dlakić, 2006). A more recent study verified that the DUF283 domain from hDicer is capable of binding single-stranded nucleic acid (Kurzynska-Kokorniak et al., 2016). The PAZ domain, conserved with respect to the same domain in Argonaut proteins, is responsible to anchor the 3′ 2 nt overhanging end of a duplex RNA substrate (Tian et al., 2014).

The multi-domain nature of hDicer lends versatile regulatory mechanisms to its nuclease activity. The DExD/H-box helicase domain causes an auto-inhibition of hDicer (Ma et al., 2008). It has been reported that hDicer-associated proteins, including TRBP, PACT, and ADAR1, bind to the DExD/H-box helicase

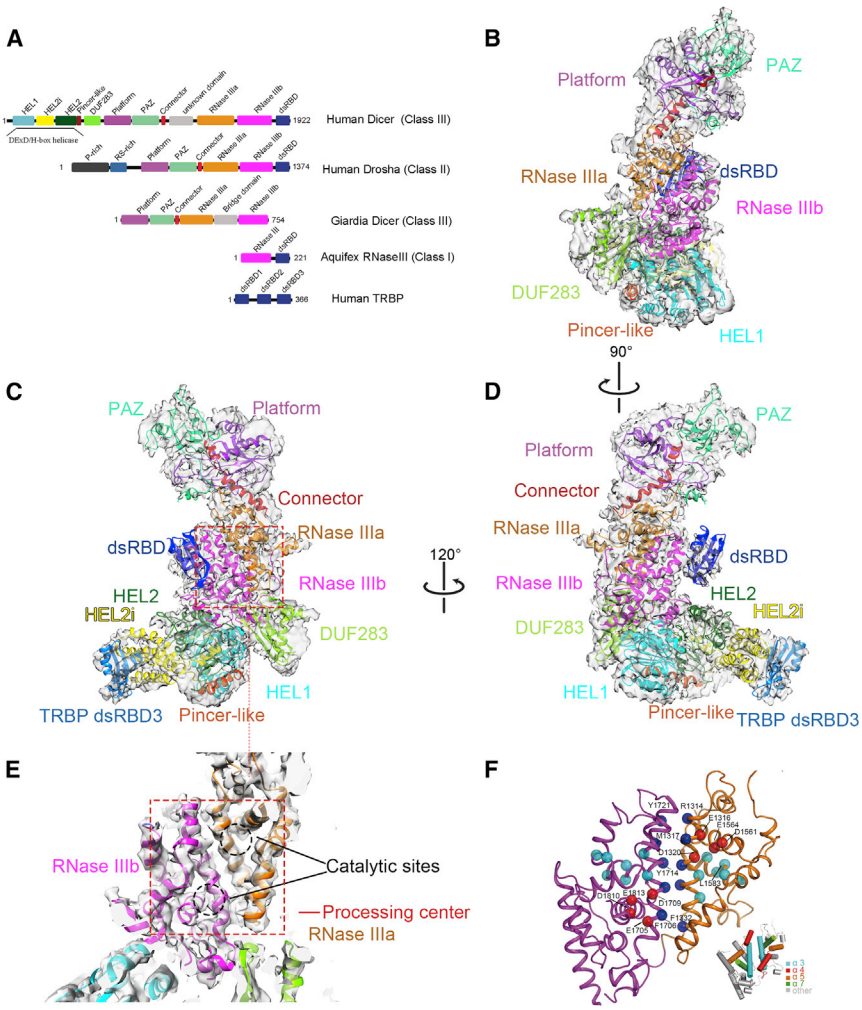

Figure 1. Cryo-EM Structure of hDicer in Complex with TRBP

(A) Schematic illustration of the domain arrangement of RNase III members and TRBP.

(B–D) The overall cryo-EM structure of the hDicer-TRBP complex. The complex exhibits an L-shaped architecture that is shown at different angles.

(E) A zoomed-in view of the processing center showing RNase III ab dimeric domains and the catalytic centers.

(F) Cartoon model of hDicer's RNase III intramolecular dimer with the Cα atoms of important residues labeled as spheres. The residues involved in the dimerization of two RNase III domains are in blue, and the residues composing the catalytic sites are in red. The cyan spheres represent the residues comprising the hydrophobic cores of each RNase III domain. Among them, L1323, I1327, A1579, L1581, F1582, L1583, and L1586 are for the RNase IIIa domain, and I1716, L1721, V1830, W1831, V1833, P1836, M1837, M1838, P1840, L1841, and I1842 are for the RNase IIIb domain. A cylinder topology of hDicer's processing center is shown at the right-bottom corner. The four most conserved helices are highlighted with different colors following the nomenclature of AaRNase III. See also Figures S1, S2, and S3.

domain and regulate hDicer's dicing activity as well as substrate selection and the cleavage site of pre-miRNAs (Chendrimada et al., 2005; Daniels et al., 2009; Lee et al., 2006; Wilson et al., 2015; Das and Carmichael, 2007; Ota et al., 2013). The structure of RNA substrates also affects hDicer's activity and site selection (Gu et al., 2012; Ma et al., 2008).

Despite all these functional and biochemical studies, the lack of a high-resolution structure of the full-length hDicer remains a major hurdle in understanding its processing mechanism. Until now, limited structural knowledge of hDicer has been obtained mainly from crystal structures of its RNase III homologs, domain fragments, and low-resolution EM reconstructions. These include the structure of *Aquifex aeolicus* RNase III (AaRNase III) enzyme mutant Aa-D44N bound to RNA at 2.05 Å resolution (Gan et al., 2006), *Giardia intestinalis* Dicer (GiDicer) at 3.33 Å resolution (Macrae et al., 2006), and human Drosha (hDrosha) in complex with the C-terminal helix of DGCR8 at 3.2 Å resolution (Kwon et al., 2016). Several individual domains of hDicer have also been successfully determined by X-ray crystallography (Takeshita et al., 2007; Tian et al., 2014; Wilson et al., 2015). Our group and others have used single-particle electron microscopy to reconstruct hDicer at ~20 Å resolution revealing its preliminary architecture as an L-shaped molecule (Lau et al., 2009, 2012; Taylor et al., 2013; Wang et al., 2009). The structure of a full-length hDicer, which is three times of a GiDicer's molecular weight and represents the largest and the most complex member of the RNase III family, still awaits to be solved toward a thorough understanding of the enzyme's mechanism.

Using single-particle cryoelectron microscopy (cryo-EM) reconstruction, we solved the structure of hDicer-TRBP complex at a near-atomic resolution and built an atomic model of hDicer. We also obtained reconstructions of the hDicer-TRBP complex bound with pre-let-7 RNAs in two distinct conformations, one with an intact stem duplex and the other with the stem partially splayed. Combined with RNase protection and RNA-probing assays, these structures revealed a function of the hDicer-TRBP complex in stabilizing the stem duplex of pre-let-7 in a substrate-loading state. Guided by the structural information, we performed biochemical analysis of hDicer's activities and revealed a unique regulatory mechanism of the protein's DExD/H-box helicase domain in the pre-miRNA processing.

RESULTS

Structure of hDicer-TRBP Complex

Human Dicer-TRBP complex with cleaving activity was expressed and purified from 293F cells (STAR Methods; Figure S1).

We succeeded to embed the complex particles in vitreous ice with optimal thickness and collected cryo-EM datasets (STAR Methods; Figure S2A) to obtain a 3D reconstruction of the hDicer-TRBP complex with an average resolution of 4.4 Å (gold-standard Fourier shell correlation at 0.143) (Figure S2). Although a few peripheral regions of the complex are limited to lower resolution due to potential flexibility, the complex's core region is well defined. The overall L-shaped architecture of hDicer-TRBP with fine detail allowed us to determine the accurate 3D positions of most folded domains within hDicer and build atomic models within them (STAR Methods; Figures S1, 1B, 1C, 1D, and S2; Movie S1). The residues 1074–1287 and residues 1378–1552 of hDicer are undetermined because of the high flexibility of these fragments (Figure S3A).

The multiple domains of hDicer (Figure 1A) arrange in a rather peculiar topology as revealed in the structure (Figures 1B–1D). Consistent with previous studies (Lau et al., 2012; Taylor et al., 2013; Wang et al., 2009), the N-terminal DExD/H-box helicase domain occupies the bottom part of the L-shaped structure of hDicer, the PAZ domain sits on the top part of hDicer, whereas the C-terminal RNase III domains form an intramolecular dimer in the middle of the molecule (Figures 1C and 1E). The DUF283 domain sits around the joint between the two arms of the L-shaped protein and has an αββββα fold resembling a dsRBD domain (Figures 1B and S4A). Through a long linker of ~40 residues, which can be modeled to fit in an obvious but poorly resolved density extending along the side of RNase IIIa domain (Figures S3B and S3C), the DUF283 domain is connected to the Platform domain and PAZ domain on the top of the L-shaped structure. A Connector α helix motif that is conserved in GiDicer and hDrosha runs through the whole Platform domain to fix the PAZ domain at one end of the Connector helix (Figures 1B, 1C, 1D, and S4C). The other end of the Connector links to a region of unknown function, corresponding to residues 1074–1287, sitting on the back of the L-shaped molecule close to the RNase IIIa domain. This unknown region, potentially facilitating the interaction between the RNase IIIa and the Platform domains, is visible in some 2D class averages but not well defined in the 3D reconstruction, indicating its flexible nature (Figures S3D and S3E). Another segment of residues (1378–1552) as an insertion within the RNase IIIa domain is too flexible to be identified in the EM map (Figure S3F). Likewise, a flexible property applies to the very C-terminal dsRBD that emanates from the RNase IIIb domain in the middle of the protein (Figure 1D). This domain lacks a clear indication of its orientation, suggesting its potential role in recruiting RNA substrates. In summary, the processing center (RNase IIIab dimer) is located in the middle of the hDicer molecule with multiple domains surrounding it, providing ample regulatory possibilities of the enzyme (Figures 1C and 1E).

TRBP is hDicer's cofactor protein and is made up of three tandem dsRBD domains (Figure 1A), and biochemical data have demonstrated that the third dsRBD domain interacts with Dicer's DExD/H-box helicase domain (Daniels et al., 2009). Our 3D reconstruction shows an obvious density corresponding to TRBP's third dsRBD domain attached to the very tip of hDicer's DExD/H-box helicase domain, whereas the other portions of TRBP are not resolved (Figures 1C and 1D). This further confirms that the tandem dsRBDs of TRBP do not associate with each other, and that they have high degrees of freedom in facilitating RNA-substrate recruitment to hDicer.

Comparison between Human Dicer and Other RNase III Family Members

Human Dicer shares similar C-terminal domains with its RNase III homologs but differs in the composition of the N-terminal regions (Figure 1A). In agreement with the high level of sequence-conservation of the RNase IIIa and IIIb domains among homologous proteins (Mendeley Data Figure 1B, https://doi.org/10.17632/bkz8c3js49.1), the atomic models of the dimeric RNase III domains from typical RNase III family members can be superimposed with an average root-mean-square deviation (RMSD) of only 1.51 Å (Figure S4B). In each of the RNase III domains, eight typical α helices that compose the RNA catalytic center are highly conserved both in secondary and tertiary structures (Figure S4A and Mendeley Data Figure 1B, https://doi.org/10.17632/bkz8c3js49.1). A hydrophobic core formed by the eight α helices in each RNase III domain is likely responsible to maintain the structure (Figures 1D, 1E, 1F, and S4B). It is worth noting that L1583 at the center of the RNase IIIa domain's hydrophobic core, when mutated to arginine, causes Familial Pleuropulmonary Blastoma (Hutvágner et al., 2001), probably due to a disruption of the protein's native fold. The RNase IIIa and IIIb domains of hDicer form an intramolecular dimer mainly through a hydrophobic lateral interaction between the two antiparallel α3 helices of each domain, where hydrophobic residues including M1317, F1332, F1706, Y1714, and Y1721 intertwine with each other (Figures 1F and S4A). These interactions maintain a highly conserved spatial arrangement of the RNase catalytic sites composed of residues E1316, D1320, D1561, and E1564 of the RNase IIIa domain and residues E1705, D1709, D1810, and E1813 of the RNase IIIb domain to cleave a dsRNA into a product with precise 2 nt 3′ overhang (Figure 1F). This emphasizes the fidelity of the RNase III active center through evolution.

Superposition of the atomic models of hDrosha, GiDicer, and hDicer in their RNase III domains unveils both common and distinct structural features within these eukaryotic homologs. All three proteins have a Connector α helix that links the RNase IIIa domain to the PAZ domain (Figures S4C and S4D). These Connector helices have a similar length of 30 amino acids (~45 Å), and they are all encircled by the Platform domain. The Connector α helix adopts almost the same structure in hDicer and hDrosha but bends to a different direction in GiDicer (Figure S4C). This causes a different PAZ domain orientation between hDicer and GiDicer, implying different RNA-processing patterns by them (see Discussion later). Around the intramolecular RNase III dimeric processing center, hDicer has a C-terminal dsRBD domain connected to the RNase IIIb domain and a dsRBD-like DUF283 domain sitting at a symmetric position, close to the RNase IIIa domain (Figure S4D). This spatial arrangement is similar to that of the AaRNase III dimer (Figure S4D). In contrast, hDrosha has only one dsRBD at the C terminus and GiDicer has no dsRBD (Figure S4D). Such an architecture surrounding hDicer's processing center implies a possible mechanism by which recruitment and processing of dsRNA substrates is regulated via the dsRBD and DUF283 domains, similar to what has been proposed in the AaRNase III dimer.

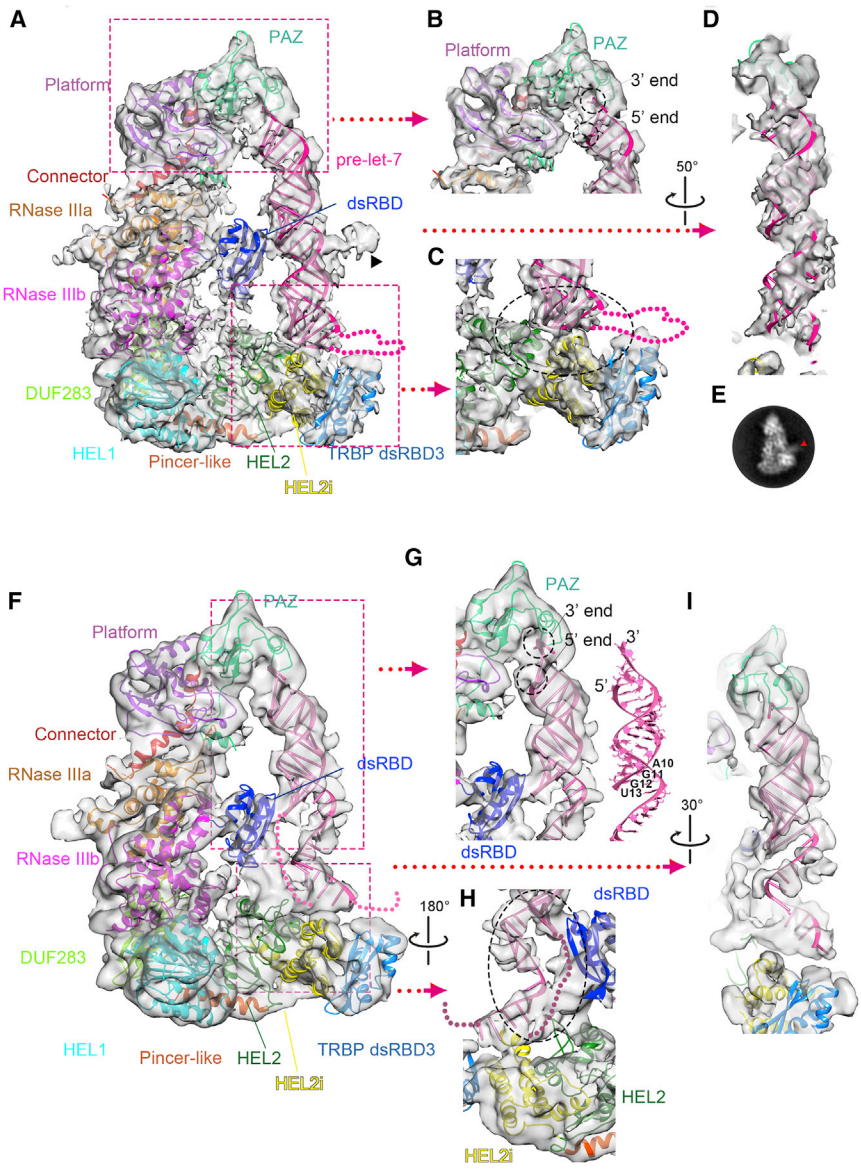

Figure 2. Cryo-EM Structure of the Ternary Complex of hDicer-TRBP-Pre-let-7

(A) The Cryo-EM structure of the hDicer-TRBP-pre-let-7 complex in class I conformation with an intact RNA stem duplex, shown in transparent surface rendering with the atomic model fitted into the density. The RNA model is shown in deep pink. The black triangle points to an unassigned density attached to the stem of pre-let-7.

(B) Close-up view shows the interaction between the Platform-PAZ-Connector cassette and the hairpin end of pre-let-7 RNA within the class I reconstruction. The 3′ end and 5′ end of pre-let-7 are marked by black circles.

(C) Close-up view shows the interface between pre-let-7 and the DExD/H-box helicase domain. The interface between the RNA and the helicase domain is marked by the dashed oval.

(D) The whole RNA stem adopting an A-form helix.

(E) A typical 2D class average showing the density (marked by red arrowhead) corresponding to the terminal loop of pre-let-7.

(F) The Cryo-EM structure of the hDicer-TRBP-pre-let-7 complex in class II conformation with the RNA stem splayed, shown in transparent surface rendering with the atomic model fitted into the density.

(G) Close-up view shows the interaction between the Platform-PAZ-Connector cassette and the hairpin end of pre-let-7 RNA within the class II reconstruction. The positions of nucleotides near the strand-separation region are marked in the RNA model.

(H) Close-up view shows the separated portion of pre-let-7's stem and the interface between the terminal loop and the DExD/H-box helicase domain (marked by the dashed oval).

(I) The splayed RNA is shown in a front view of the map.

See also Figure S5.

Structure of hDicer-TRBP in Complex with Pre-let-7

In order to better understand hDicer's interaction with its RNA substrates, the hDicer-TRBP-pre-let-7 complex was assembled in a buffer containing Ca^{2+}, which maintains the protein-RNA interaction but inhibits the dicing activity (Figure S1C). Cryo-EM analysis of the hetero-trimeric complex revealed the co-existence of two dominant conformers that shared a very similar structure to that of the hDicer-TRBP portion but demonstrated distinct RNA densities bound to the protein (Figures 2 and S5). In one reconstruction at 4.7 Å resolution, the RNA density adopts an intact stem duplex for pre-let-7 (class I); in the other reconstruction at 5.7 Å, the density corresponding to the pre-let-7 stem is partially splayed (class II) (Figures 2 and S5 and Movie S2). The ratio of particle numbers between the two classes is 2:1.

In the class I reconstruction, a right-handed spiral-like density, spanning between hDicer's PAZ domain and the DExD/H-box helicase domain, shows clear major and minor grooves, accommodating a predicted 3D model of pre-let-7 with an A-form dsRNA stem structure (Figures 2A–2D, 3E, and S5). Consistent with previous biochemical and structural data (Macrae et al., 2006; Tian et al., 2014; Tsutsumi et al., 2011), the 3′ end of pre-let-7 fits in the 3′ end binding pocket within the PAZ domain (Figure 2B). Interestingly, the 5′ end of pre-let-7 does not interact with the PAZ domain in our structure. The other end of the RNA stem can be clearly identified to interact with hDicer's DExD/H-box helicase domain (Figures 2A, 2C, and 2D). Although the density corresponding to the terminal loop of pre-let-7 is not well defined in the 3D map, the pre-let-7 model can be roughly oriented by 2D class averages of the complex, where signal for the pre-let-7 terminal loop can be detected (Figure 2E). In addition to the PAZ and DExD/H-box domains serving to anchor pre-let-7 from the two ends, the dsRBD holds the middle portion of pre-let-7 (Figure 2A). Such a configuration of pre-let-7 in the complex keeps the RNA in a

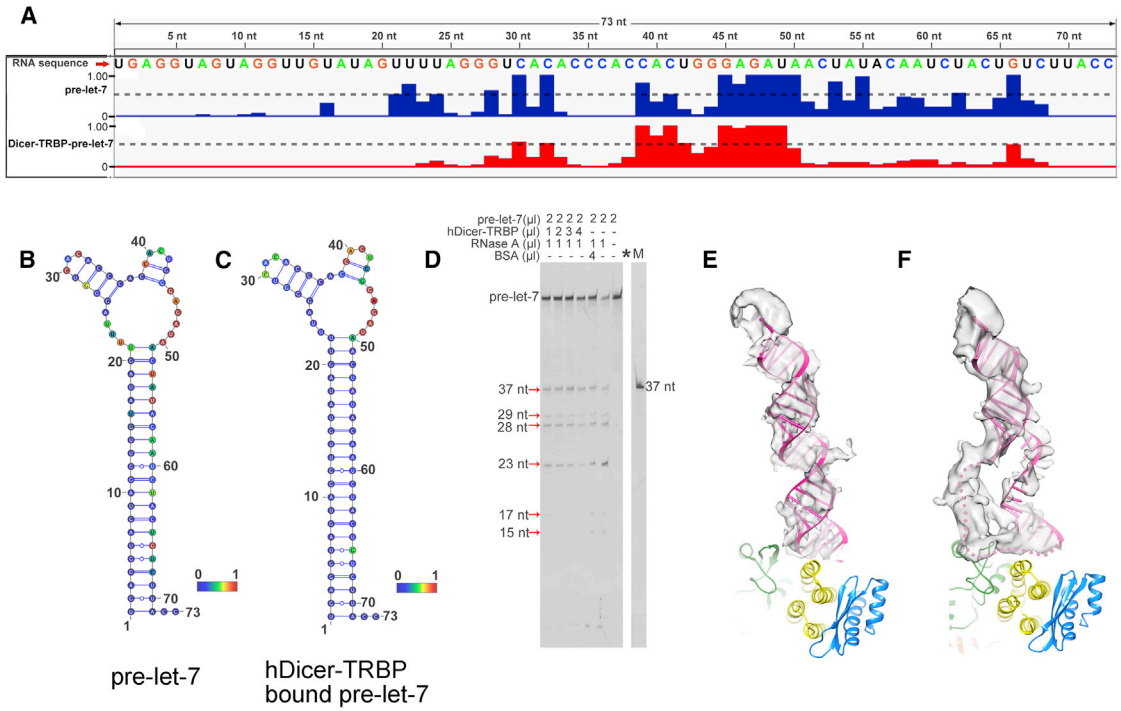

Figure 3. Secondary Structural States of Pre-let-7 RNA

(A) The icSHAPE analysis to probe the free nucleotides of pre-let-7 in free and hDicer-TRBP-bound states, respectively.

(B and C) The RNA-probing results of pre-let-7 shown in a predicted secondary structure model in the free and hDicer-TRBP-bound states, respectively. Red circles represent the most active nucleotide sites, and blue circles label the least active nucleotide sites.

(D) RNase A digestion pattern of 5′ FAM-labeled pre-let-7 pre-assembled with hDicer-TRBP. * refers to the removed unnecessary lanes.

(E and F) The model of RNAs traced in the EM density of hDicer-TRBP-pre-let-7 class I and class II conformations, respectively.

See also Figure S6.

position away from the RNA-processing center, implicating a possible substrate-loaded state of hDicer before the dicing reaction.

In the class II reconstruction, the protein portion maintains the same structure as in class I reconstruction. The first 12 bp of pre-let-7 stem (counted from 5′ termini) also adopts a very similar shape as in class I reconstruction (Figure 2G). The second half of the stem, however, shows an unexpected feature of separation of the two RNA strands in pre-let-7's stem region from the 13th nt (counted from the 5′ termini) (Figures 2F–2I, and 3F). The terminal loop of pre-let-7 cannot be modeled in the EM density at all, implying its high-flexibility nature. The interface between the pre-let-7 RNA and hDicer's DExD/H-box helicase domain also adopts different shape in this reconstruction than in class I reconstruction (Figure 2H). This suggests that hDicer's DExD/H-box helicase domain has a high tolerance to various RNA-terminal loop structures.

The cryo-EM reconstructions also illustrate TRBP's interaction with hDicer and the RNA substrate. As expected, in the 3D maps of the hDicer-TRBP complex and the hDicer-TRBP-pre-let-7 complex, the interaction between the third dsRBD domain of TRBP and HEL2i is clearly resolved. In contrast, the first two dsRBD domains cannot be unambiguously defined in the 3D maps, although some sporadic densities surrounding the dsRNA stem of pre-let-7 within the reconstructions could be detected potentially corresponding to the dsRBDs (Figures 2A and S5E). There is also a noticeable bulge density attached to the middle of the RNA stem of class I reconstruction possibly corresponding to one of the two dsRBDs (Figure 2A). This agrees with a previous model that the long-range flexibility of TRBP allows it to capture and feed RNA substrates to the RNA-interacting functional groups in Dicer through the first two dsRBDs but may not necessarily bind the RNA substrates in a well-defined manner.

The two reconstructions illustrated that the hDicer-TRBP complex can load at least two different conformers of pre-let-7 RNA with either an intact stem duplex or a partially separated stem beyond the first 13 bp. On the other hand, however, the dicing reaction of hDicer-TRBP on pre-let-7 produced a precise 22 bp product when Mg^{2+} was introduced into the pre-reconstituted hDicer-TRBP-pre-let-7 complex (Figure S6B). These seemingly contradictory experimental results led us to investigate the structural variation of pre-let-7 in the presence and absence of the hDicer-TRBP complex.

Stabilization of Pre-let-7's Stem Duplex by hDicer-TRBP Complex

Our observation of two different conformers of pre-let-7 RNA in the hetero-trimeric complex made us wonder whether the RNA conformational variation is an intrinsic property of the free pre-let-7 RNA or induced by the hDicer-TRBP complex. Because

an in vitro synthesized and refolded pre-let-7 RNA substrate was used in all the experiments in this work, we performed biochemical characterization of the RNA, verifying its chemical homogeneity and proving that it can be precisely diced into a 22 bp product (Figures S6A and S6B). Although pre-let-7 can be predicted as a hairpin structure with a stem duplex and a loop in the middle, there is no experimental structure of the RNA by itself.

We used a combinational approach of RNase-limited digestion and RNA probing to analyze the secondary structures of the RNA in the absence and presence of the hDicer-TRBP complex. We used the endonucleases RNase T1 and RNase A, which specifically cleave G and U/C, respectively, within single-stranded RNAs, to digest free pre-let-7 in the presence of Mg^{2+}. As expected, we observed some clear cleavage patterns within the predicted loop region of the RNA (G25, G26, G27, U29, C30, C38, G44, G45, G46, G47) (Figures S6C and S6D). Some unexpected cleavage patterns were observed within the predicted stem region (U9, U16, U18, G20), indicating a separation of the RNA strands within the stem. This behavior of pre-let-7 was further confirmed in an RNA probing assay that used NAI-N3 to probe the single-stranded nucleotides within RNAs (Figures 3A and 3B). These results indicated that free pre-let-7 may adopt different conformations in solution with various stem stabilities. Therefore, the different shapes of RNA in the hDicer-TRBP-pre-let-7 complex may reflect the loading of preexisting various conformers of pre-let-7. Interestingly, the pre-let-7's stem became more stable in the presence of hDicer-TRBP as revealed by the RNA-probing assay (Figures 3A–3C). Consistently, the RNase A digestion assay showed a much weaker cleavage pattern within the stem region but not the loop region when hDicer-TRBP was present (U16 and U18 in Figure 3D). These results suggested that the hDicer-TRBP complex could promote pre-let-7 into a conformation with a more stable stem duplex. Alternatively, the hDicer-TRBP complex might prefer to bind pre-let-7 conformers with a more intact stem duplex and drive the conformational equilibrium of pre-let-7 toward a stable state. Therefore, the class I reconstruction of the hDicer-TRBP-pre-let-7 complex probably represents a pre-dicing state of pre-miRNA.

Structural Basis for RNA Cleavage-Site Selection by hDicer

We compared the interaction between the pre-let-7's hairpin end and hDicer's PAZ domain in our class I structure of the hDicer-TRBP-pre-let-7 complex with the previously solved crystal structures of hDicer's Platform-PAZ-Connector helix cassette in complex with short siRNAs (Tian et al., 2014). We found that the protein portion of the cassette in our cryo-EM structures is very similar to that of the cassette bound with a 16 bp short RNA in crystals, in which the hDicer-specific helix is melted (Figures 4A and 4B). However, the RNA substrate sits in a distinct orientation in our cryo-EM structure relative to that in the crystal structure. The dsRNA in the crystal structure is positioned toward the surface of the hDicer Platform, whereas in our structure the RNA orients away from the Platform. As a result, the pre-let-7 5′ end is more than 15 Å away from the potential phosphate-binding pocket of the Platform domain in our structure (Figure 4A). It was postulated that the protein structure of the cassette with a disordered hDicer-specific helix represents a cleavage-competent state of hDicer (Tian et al., 2014). Indeed, if we adjust pre-let-7 RNA's duplex stem in the same orientation as in the crystal structure, the RNA would swing about 30 degrees and lie against the Platform and RNase III domains for cleavage (Figure 4A). The melting of the hDicer-specific helix in our structure indicates that hDicer is already in a state to bring the RNA substrate into the processing center, further supporting the notion that the class I structure may represent a substrate-loading state.

We used the crystal structures of the dimeric AaRNase III-dsRNA complex (PDB: 2EZ6) and hDicer Platform-PAZ-Connector cassette-16-mer dsRNA complex (PDB: 4NHA) to dock a model of A-form dsRNA onto the atomic model of hDicer's processing unit (Figure 4C). In such a model, the dsRNA has a 2 nt 3′-overhang binding to PAZ domain's 3′ end binding pocket and lies against the processing-unit catalytic side surface with its double-stranded stem held by the dsRBD and DUF283 domains. The model measures the distance from the 3′ end binding pocket of hDicer's PAZ domain to the RNase IIIa catalytic site as about 58 Å, shorter than the 65 Å distance for GiDicer. Based on the "3′ counting model" (Macrae et al., 2006), which hypothesizes the length of RNA product to be determined by measuring the cleavage site from dsRNA's 3′ end, the RNA products cleaved by hDicer should have a length of ~22 bp, whereas those by GiDicer are ~25 bp (Figure 4C) (Macrae et al., 2006). It is worth noting that the distance from the Platform domain's 5′ phosphate-binding pocket to the RNase IIIb catalytic site is the same length as the ~22 bp measurement, therefore also supporting the "5′ counting model" (Park et al., 2011).

Features of hDicer's DExD/H-Box Helicase Domain

Our structures of pre-let-7 bound to hDicer in an incompetent state indicate an important regulatory role by the terminal loop-binding domain, the DExD/H-box helicase domain, in the dicing reaction. Sequence alignment suggests that hDicer's DExD/H-box helicase domain is highly homologous to that of the RIG-I family of RNA helicase (Figure S7B and Mendeley Data Figure 2, https://doi.org/10.17632/bkz8c3js49.1) (Zou et al., 2009). Based on the homology analysis, we further divided the DExD/H-box helicase domain into three domains: HEL1, HEL2i, and HEL2 (Figures 5A and 5B). The whole DExD/H-box helicase domain exhibits a C-shaped structure composed of three discrete domains with an arrangement similar to those of the RIG-I (Figures 5B–5D) (Kowalinski et al., 2011). The very N-terminal HEL1 is located at the junction between the arms of the L and interacts with DUF283 and the RNase IIIb domains. HEL2 is positioned at the center of the C-shaped arrangement, whereas HEL2i sits at the tip of the short arm of the L. Both the HEL1 and HEL2 domains are characterized by four or five β strands surrounded by several α helices, and the HEL2i domain is featured by four antiparallel α helices that interact with the third dsRBD of TRBP (Figures 5B and 5C), in agreement with previous results (Wilson et al., 2015).

Besides the similar structure and spatial arrangement of the helicase domains of hDicer and RIG-I, a prominent α helix connecting the HEL1 and HEL2 domains exists in both proteins (Figures 5B, 5D, and 5E). This α helix is part of a two-stretch helix in RIG-I, known as the pincer motif, so we call it a pincer-like motif

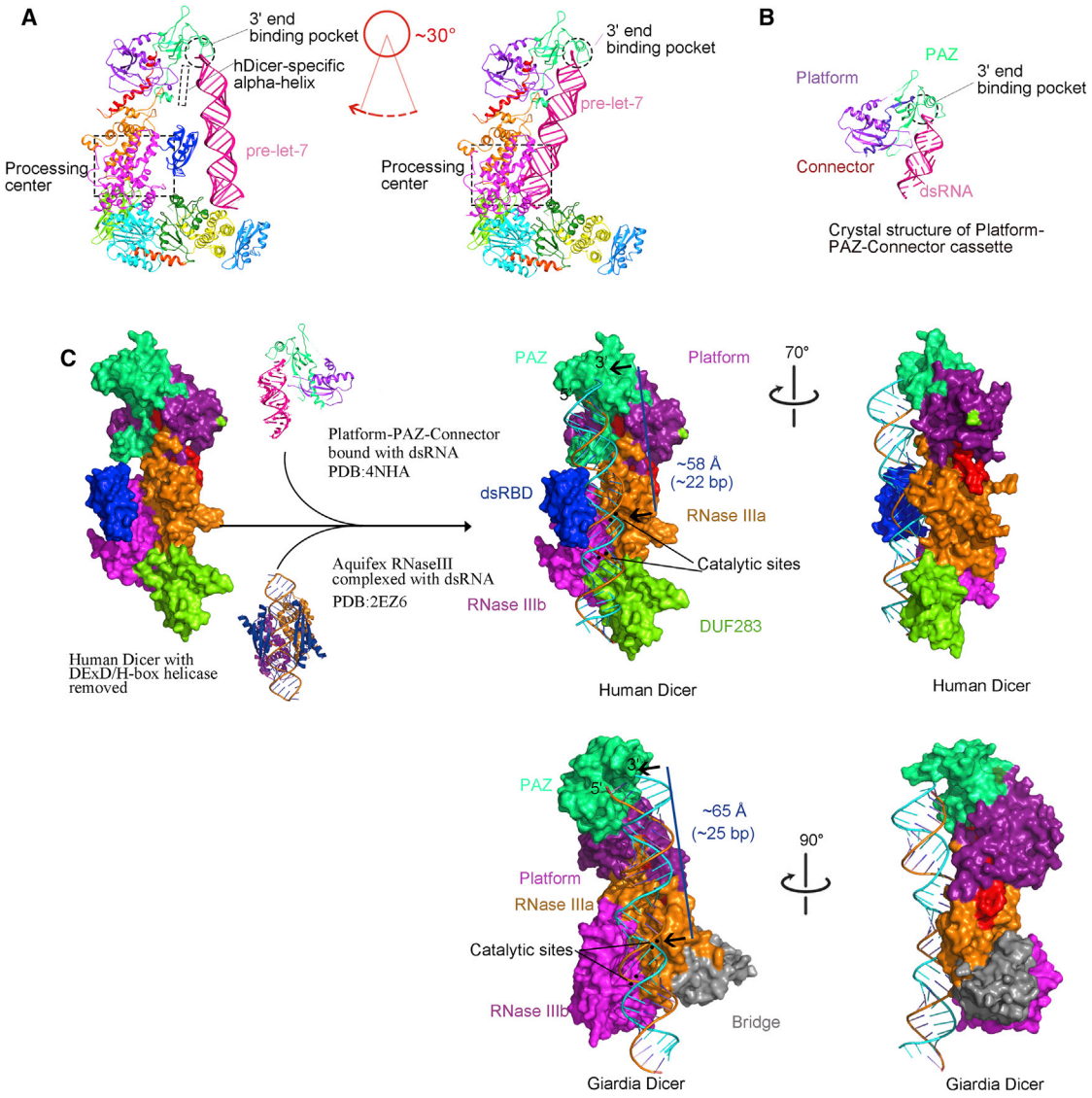

Figure 4. Analysis on the Interplay between Pre-let-7 and hDicer

(A) The atomic model of the hDicer-TRBP-pre-let-7 complex is shown (left panel). A modeled structure of hDicer-TRBP-pre-let-7 was obtained by reorienting the pre-let-7 RNA to align with the 16-mer siRNA in the crystal structure of the Platform-PAZ-Connector cassette (PDB: 4NHA) (right panel). The potential location of the hDicer-specific α helix in the PAZ domain is marked by a dashed rectangle. The processing center is marked with a dashed red rectangle. The 3′ end RNA-binding pocket of the PAZ domain is labeled by a red circle.

(B) The crystal structure of the Platform-PAZ-Connector cassette bound with 16-mer dsRNA (PDB: 4NHA).

(C) Schematic drawing of the way in which we modeled dsRNA into hDicer's processing unit. Surface representation of the atomic model of hDicer's processing unit with a model of dsRNA bound at the catalytic site is shown in two different views. The catalytic sites are marked by pairs of black dots; black arrows illustrate the distances between the 3′ end of dsRNA and the corresponding cleavage site of the same strand; the two strands of the dsRNA are colored in cyan and orange colors, respectively.

in hDicer (Figures 5B and 5C). The pincer motif of RIG-I allows the HEL1 domain to adopt variable angular movement around the HEL2 and HEL2i modules in the ligand-free state (Zou et al., 2009). As a matter of fact, when we performed further classification of the apo-hDicer-TRBP complex dataset around the DExD/H-box helicase domain, we obtained two major conformers of the complex sharing the same structure for their C-terminal regions but differing slightly in the orientation of their N-terminal helicase domains (Figure 5C), which indicated a flexible nature of this region (Figure S2). Close inspection of the two reconstructions confirmed our previous observation that hDicer's HEL2 and HEL2i modules (the short arm of "L") show strong flexibility around the HEL1 domain (Taylor et al., 2013). A comparison between the RIG-I helicase domains and hDicer helicase domains indicates the presence of highly conserved residues distributed on the concave surface of the C-shaped

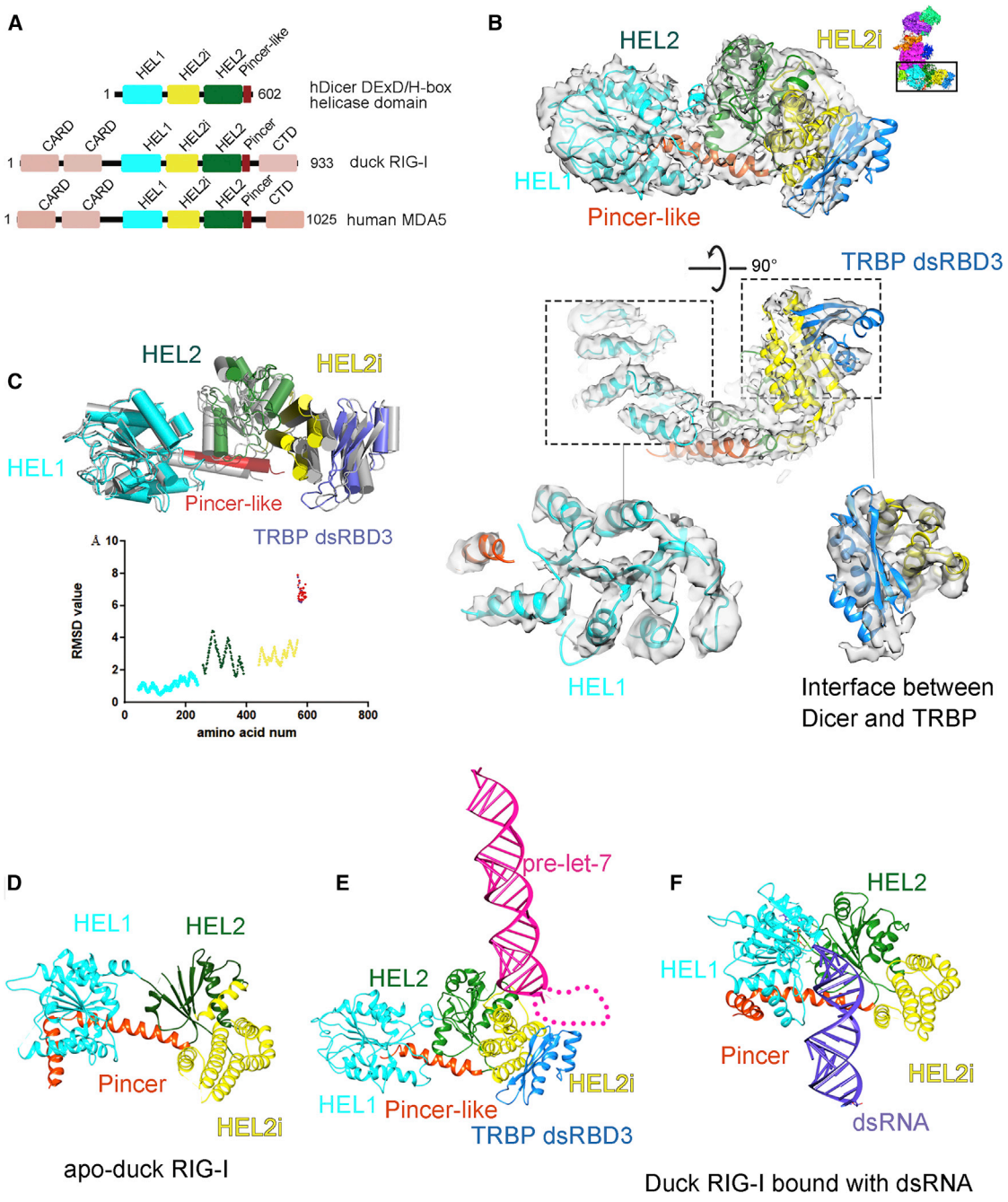

Figure 5. Structure of the DExD/H-Box Helicase Domain of hDicer

(A) Schematic arrangement of the primary sequence of the hDicer DExD/H-box helicase domain, duck RIG-I, and human MDA5.

(B) The DExD/H-box helicase domain cryo-EM density with the corresponding atomic model fitted into the density, shown in orthogonal views as illustrated by the insets. The HEL1 domain is in cyan, the HEL2i domain in yellow, the HEL2 domain in forest green, and the Pincer-like motif in orange red. The third dsRBD of TRBP is in blue.

(C) Two conformations of the DExD/H-box helicase domain of the apo-hDicer-TRBP complex based on the 3D classification are superimposed with the HEL1 domains aligned. The RMSD values of different residues to demonstrate the variation of the HEL1, HEL2i, HEL2, and Pincer-like domains are shown in the lower panel.

(D) Structure of duck RIG-I in an inactive state (PDB: 4A2P) shown in the same view as in (B) and (C).

(E) Structural model of the hDicer DExD/H-box helicase domain bound with the pre-let-7 RNA extracted from our cryo-EM structure of the the hDicer-TRBP-pre-let-7 complex.

(F) Structure of duck RIG-I in active state upon binding to dsRNA (PDB: 4A36).

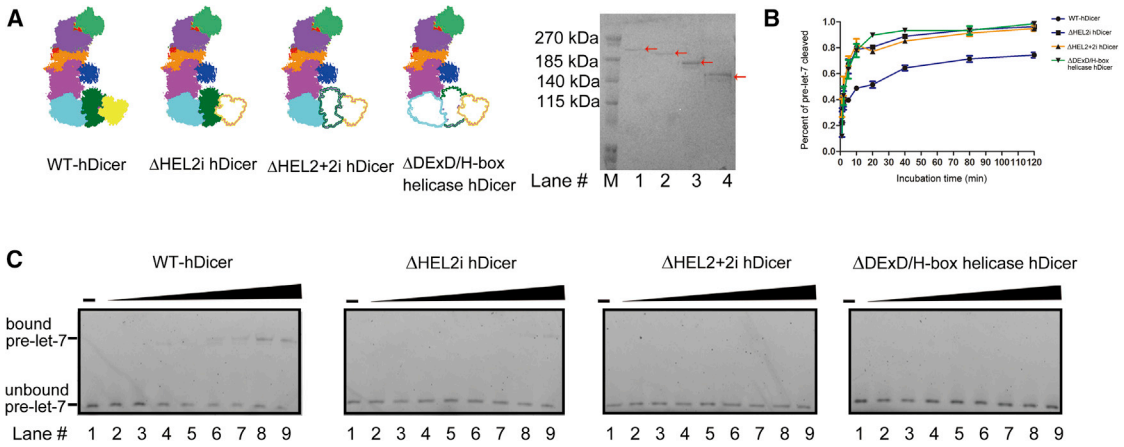

Figure 6. Dicing Activities and RNA-Binding Affinities of Various DExD/H-Box Helicase Domain Truncation Mutants

(A) Illustration of truncated hDicer proteins and their SDS-PAGE analysis.

(B) Dicing activities of the different truncated constructs. Error bars represent SD.

(C) Binding affinities of the different truncated constructs on pre-let-7.

See also Figure S7.

structure, which also interact with dsRNA substrates in RIG-I (Figures 5F and S7B) (Kowalinski et al., 2011). Unexpectedly, the interface between the terminal loop of pre-let-7 and hDicer's DExD/H-box helicase domain within our hDicer-TRBP-pre-let-7 structure is not located on the concave surface of the C-shaped structure but on the boundary surface between HEL2i and HEL2 (Figure 5E). The boundary surface is mostly positively charged and highly conserved among Dicer proteins in higher organisms, in agreement with its property to bind the terminal loop of pre-let-7 RNA (Figure S7C and Mendeley Data Figure 3, https://doi.org/10.17632/bkz8c3js49.1).

The stable interaction between pre-let-7 and the DExD/H-box helicase domain in a dicing-incompetent state indicates two seemingly contradictory functions of the helicase domain: recruiting RNA substrates and inhibiting cleavage. We generated truncated hDicer constructs based on our structural model to investigate the roles of helicase domains in the RNA-dicing reaction (Figure 6). As predicted, the deletion of helicase domains consecutively from the tip of the short arm of L-shaped hDicer dramatically reduced the binding affinity for pre-let-7 RNA (Figure 6C). Interestingly, the dicing activity was enhanced in all the truncated mutants (Figures 6B and S7A). From an enzymatic point of view, the reduction of RNA's binding affinity is not necessarily accompanied with a reduction of the catalytic activity in the helicase domain truncated mutants. What we observed for the enhanced dicing activity of the mutants is an indicator that the dicing step might be a fast and transient process in hDicer's processing center. The high structural similarity and conservation of the hDicer's helicase domain with that of RIG-I suggests a potential process in which the pre-let-7's terminal loop transverses between the boundary surface formed by the HEL2i and HEL2 domains and the concave surface of the C-shaped DExD/H-box helicase domain. Indeed, in a dicing-reaction condition with magnesium for pre-let-7, hDicer adopted major conformational changes in the DExD/H-box helicase domain (Figures S7D and S7E).

DISCUSSION

Our reconstructions of hDicer-TRBP and hDicer-TRBP-pre-let-7 complexes allowed us to dissect the complexes as intact molecules and build an atomic model of the core processing unit and the N-terminal DExD/H-box helicase region of hDicer. Notwithstanding, there are still more than 500 aa residues of the protein that cannot be determined due to the flexible nature of the molecule (Figure S3A). Solution of the structure of full-length hDicer at atomic resolution is still a very challenging task.

The crystal structure of dsRNA-bound AaRNase III revealed that a catalytic center is formed by a homodimer of two RNase III domains and two dsRBDs (Gan et al., 2006). Human Dicer has a catalytic center formed by the intramolecular dimerized RNase IIIa and IIIb domains that mimics the homodimer of AaRNase III (Figure S4D). The C-terminal dsRBD and DUF283 domain within hDicer are located around the catalytic center in a similar fashion as with the two dsRBDs in the AaRNase III dimer (Figure S4D). Moreover, the non-catalytic assembly of the AaRNase III-dsRNA complex and the AaRNase III-product complex placed the RNA substrates and products in different locations (Blaszczyk et al., 2004; Gan et al., 2006), indicating that the dsRBD and DUF283 domain within hDicer could play similar roles to those of the dsRBDs of AaRNase III dimers to switch RNA substrates and products during the reaction.

Until now, there has been no experimental 3D structure of any pre-miRNA in its free state. Our work here suggested that pre-let-7 RNA, at least through in vitro synthesis and refolding, may adopt multiple conformations in solution as well as bound to the hDicer-TRBP complex. Whether this is a general property of other pre-miRNAs, especially in vivo, will need further study. But it may provide a possible mechanistic explanation of certain regulations via stem modification of pre-miRNAs such as the A-to-I edition. Given that no major conformational difference were observed within the protein region between the two hDicer-TRBP-pre-let-7 complex reconstructions at current

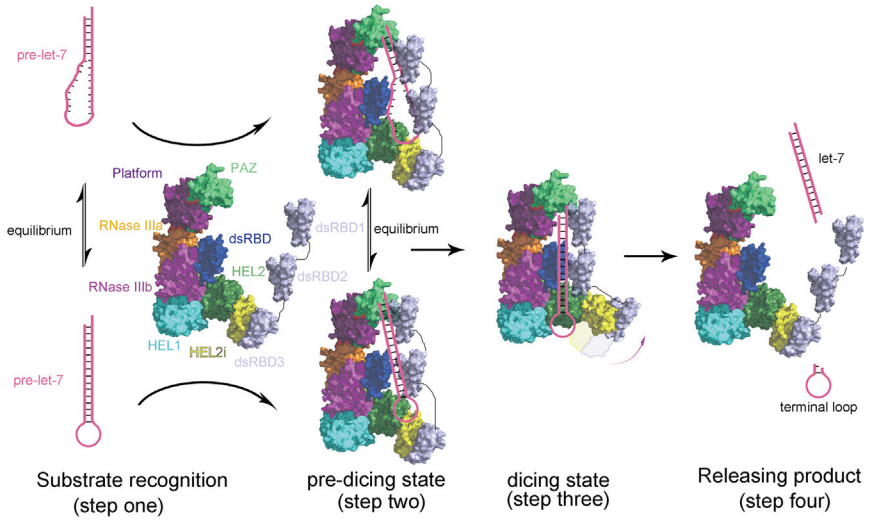

Figure 7. A Hypothetical Model of Pre-miRNA Processing by hDicer

Human Dicer recruits pre-let-7 in different conformations with the aid of TRBP. The hDicer-TRBP complex can promote the stability of pre-let-7's stem duplex in a pre-dicing state. The pre-let-7 is loaded into hDicer's processing center for precise dicing reaction by a potential major conformational change of the DExD/H-box helicase domain. After dicing, the cleaved products are released from the hDicer-TRBP complex. The dsRBD1 and dsRBD2 of TRBP bound to the RNA are not based on the experimental data but only shown as a demonstration.

resolution, we cannot tell for sure what structural elements are responsible for this kind of promotion. The protein complex may simply serve as an RNA chaperon to facilitate the RNA's conformational shift. It is worth noting that there are more than 1,800 species of pre-miRNAs (Griffiths-Jones, 2004, 2006). The promotion of pre-miRNAs with various sequence and secondary structural compositions into a stem duplex before dicing would provide a convenient mechanism for hDicer's precise measurement of the substrates for dicing. Higher resolution of the structures may provide more detail of the mechanism in the future.

The DExD/H-box helicase domain located at the bottom of hDicer's processing center lends the enzyme more complicated RNA transaction behaviors than prokaryotic RNase III and GiDicer. Our structure of the pre-let-7-bound hDicer-TRBP complex showed an interaction between pre-let-7's terminal-loop region and the DExD/H-box helicase domain, implying that the structure of pre-miRNA's terminal loop may influence hDicer's RNA-dicing activity via potential allosteric effects by both the protein and/or the RNA molecule. These observations may also reflect another RNA cleavage-site selection mechanism, via the terminal loop, termed the "loop-counting model" (Gu et al., 2012). The DExD/H-box helicase domain also serves as a platform for hDicer to bind to TRBP, which was shown previously to alter the cleavage pattern of pre-miRNAs (Lee and Doudna, 2012) and recruit Ago2 to load small RNA products generated by hDicer (Gregory et al., 2005).

Although the structure of hDicer's dicing state on RNA substrates is still unknown, the reconstruction of the hDicer-TRBP-pre-let-7 complex presented in the current work uncovered a non-catalytic state during the reaction cycle of RNA processing by hDicer. The melt of the hDicer-specific alpha-helix in its PAZ domain in the hDicer-TRBP-pre-let7 complex suggests that hDicer is in a cleavage-competent conformation, ready to dice the RNA substrate (Figure 7). However, the N-terminal DExD/H-box helicase domain holds the terminal loop of pre-let-7 from accessing hDicer's processing center. We postulate that this structure represents a pre-dicing state immediately after loading of the RNA substrate to hDicer and adjusting the RNA's conformation for a more stable stem duplex, potentially by the help of TRBP (Figure 7). The fact that this structure dominates the single-particle population suggests it to be a relatively stable conformation. Therefore, the limiting step for RNA processing is probably the transition from this pre-dicing state to the competent catalytic state, which is likely to be accompanied by a major conformational change of hDicer and relocation of RNA substrates in the complex (Figure 7).

During this limiting step, the conformational change of hDicer may cause the dsRNA portion of the stem loop or a pre-siRNA to protrude into the conserved, concave region of the DExD/H-box helicase domain for a more rigid interaction with the RNA substrate. The helicase domains and the tandem dsRBDs of TRBP or PACT proteins may play roles cooperatively in adjusting the bound RNA substrate into the best configuration and position in hDicer's processing center, thus allowing a precise cleavage, as unveiled in earlier works (Noland et al., 2011; Taylor et al., 2013; Wilson et al., 2015). This precise positioning of the RNA substrate is then followed by a classical RNase III cleavage to generate diced small dsRNAs and a residual stem loop. Products are later released into solution or loaded to RISC complexes by a mechanism yet to be discovered (Figure 7). The difficulty to capture the active dicing state of hDicer on its RNA substrate in our experimental conditions suggests that the dicing state might be a rather fast catalytic reaction step followed by the product release. A plausible triggering mechanism of the dicing process might be caused by a Brownian-ratchet-like motion of the DExD/H-box helicase domain relative to the processing center. The energy of the reaction could come from the hydrolysis of RNA strands. The dicing state and other functional states of hDicer in small RNA biogenesis are awaiting to be further revealed both structurally and mechanistically.

STAR★METHODS

Detailed methods are provided in the online version of this paper and include the following:

- KEY RESOURCES TABLE
- CONTACT FOR REAGENT AND RESOURCE SHARING

SUPPLEMENTAL INFORMATION

Supplemental Information includes seven figures, three tables, and two movies and can be found with this article online at https://doi.org/10.1016/j.cell.2018.03.080.

ACKNOWLEDGMENTS

The plasmids of hDicer and TRBP were gifts from J. Doudna. We are thankful to J.L. Lei, Y.J. Xu, X.M. Li, and T. Yang at the Tsinghua University Branch of the China National Center for Protein Sciences (Beijing) for providing the cryo-EM and high-performance computational facility support. We also thank the "Explorer 100" High Performance Computation Facility of Tsinghua National Laboratory for Informational Science and Technology. We acknowledge the helpful advice of E. Ma, S. Sun, M.S. Ma, L. Wang, and K. Ye in the setup of protein expression and purification as well as RNA biochemistry assays. We thank J. Wang, C.Y. Yan, D.S. Liu, and Y. Wu for their guidance in model building and R.M. Glaeser and N. Yan for their careful reading of this work. This work is supported by funds from the National Science Foundation of China (Grant 31530018 to H.-W.W. and Grant 31671355 to Q.C.Z.), the National Key R&D Program of China (Grant 2016YFA0501100 to H.-W.W.), and the Beijing Municipal Science & Technology Commission (Grant Z161100000116034 to H.-W.W.).

AUTHOR CONTRIBUTIONS

H.-W.W. initiated and supervised the project. Z.L., X.K., and H.C. prepared and purified the proteins. Z.L. and J.W. prepared the cryo-EM specimens. J.W., Z.L., X.K., and H.C. collected the EM data. J.W. performed the cryo-EM analysis and the model building. Z.L. and X.K. performed the biochemical analysis in RNA dicing and RNase degradation assays. L.S. and Q.C.Z. performed the RNA-probing assay and icSHAPE analysis. H.-W.W. and Z.L. wrote the manuscript with help from all authors.

DECLARATION OF INTERESTS

The authors declare no competing interests.

Received: June 29, 2017
Revised: January 2, 2018
Accepted: March 28, 2018
Published: April 26, 2018

REFERENCES

Adams, P.D., Afonine, P.V., Bunkóczi, G., Chen, V.B., Davis, I.W., Echols, N., Headd, J.J., Hung, L.W., Kapral, G.J., Grosse-Kunstleve, R.W., et al. (2010). PHENIX: a comprehensive Python-based system for macromolecular structure solution. Acta Crystallogr. D Biol. Crystallogr. *66*, 213–221.

Ambros, V., Bartel, B., Bartel, D.P., Burge, C.B., Carrington, J.C., Chen, X., Dreyfuss, G., Eddy, S.R., Griffiths-Jones, S., Marshall, M., et al. (2003). A uniform system for microRNA annotation. RNA *9*, 277–279.

Bernstein, E., Caudy, A.A., Hammond, S.M., and Hannon, G.J. (2001). Role for a bidentate ribonuclease in the initiation step of RNA interference. Nature *409*, 363–366.

Betancur, J.G., and Tomari, Y. (2012). Dicer is dispensable for asymmetric RISC loading in mammals. RNA *18*, 24–30.

Blaszczyk, J., Gan, J., Tropea, J.E., Court, D.L., Waugh, D.S., and Ji, X. (2004). Noncatalytic assembly of ribonuclease III with double-stranded RNA. Structure *12*, 457–466.

Castilla-Llorente, V., Nicastro, G., and Ramos, A. (2013). Terminal loop-mediated regulation of miRNA biogenesis: selectivity and mechanisms. Biochem. Soc. Trans. *41*, 861–865.

Chendrimada, T.P., Gregory, R.I., Kumaraswamy, E., Norman, J., Cooch, N., Nishikura, K., and Shiekhattar, R. (2005). TRBP recruits the Dicer complex to Ago2 for microRNA processing and gene silencing. Nature *436*, 740–744.

Court, D.L., Gan, J., Liang, Y.H., Shaw, G.X., Tropea, J.E., Costantino, N., Waugh, D.S., and Ji, X. (2013). RNase III: Genetics and function; structure and mechanism. Annu. Rev. Genet. *47*, 405–431.

Daniels, S.M., Melendez-Peña, C.E., Scarborough, R.J., Daher, A., Christensen, H.S., El Far, M., Purcell, D.F., Lainé, S., and Gatignol, A. (2009). Characterization of the TRBP domain required for dicer interaction and function in RNA interference. BMC Mol. Biol. *10*, 38.

Das, A.K., and Carmichael, G.G. (2007). ADAR editing wobbles the microRNA world. ACS Chem. Biol. *2*, 217–220.

Dlakić, M. (2006). DUF283 domain of Dicer proteins has a double-stranded RNA-binding fold. Bioinformatics *22*, 2711–2714.

Du, Z., Lee, J.K., Tjhen, R., Stroud, R.M., and James, T.L. (2008). Structural and biochemical insights into the dicing mechanism of mouse Dicer: a conserved lysine is critical for dsRNA cleavage. Proc. Natl. Acad. Sci. USA *105*, 2391–2396.

Emsley, P., and Cowtan, K. (2004). Coot: model-building tools for molecular graphics. Acta Crystallogr. D Biol. Crystallogr. *60*, 2126–2132.

Filipowicz, W., Bhattacharyya, S.N., and Sonenberg, N. (2008). Mechanisms of post-transcriptional regulation by microRNAs: are the answers in sight? Nat. Rev. Genet. *9*, 102–114.

Flynn, R.A., Zhang, Q.C., Spitale, R.C., Lee, B., Mumbach, M.R., and Chang, H.Y. (2016). Transcriptome-wide interrogation of RNA secondary structure in living cells with icSHAPE. Nat. Protoc. *11*, 273–290.

Friedman, R.C., Farh, K.K., Burge, C.B., and Bartel, D.P. (2009). Most mammalian mRNAs are conserved targets of microRNAs. Genome Res. *19*, 92–105.

Gan, J., Tropea, J.E., Austin, B.P., Court, D.L., Waugh, D.S., and Ji, X. (2006). Structural insight into the mechanism of double-stranded RNA processing by ribonuclease III. Cell *124*, 355–366.

Graham, F.L., Smiley, J., Russell, W.C., and Nairn, R. (1977). Characteristics of a human cell line transformed by DNA from human adenovirus type 5. J. Gen. Virol. *36*, 59–74.

Gregory, R.I., Chendrimada, T.P., Cooch, N., and Shiekhattar, R. (2005). Human RISC couples microRNA biogenesis and posttranscriptional gene silencing. Cell *123*, 631–640.

Griffiths-Jones, S. (2004). The microRNA Registry. Nucleic Acids Res. *32*, D109–D111.

Griffiths-Jones, S. (2006). miRBase: the microRNA sequence database. Methods Mol. Biol. *342*, 129–138.

Gu, S., Jin, L., Zhang, Y., Huang, Y., Zhang, F., Valdmanis, P.N., and Kay, M.A. (2012). The loop position of shRNAs and pre-miRNAs is critical for the accuracy of dicer processing in vivo. Cell *151*, 900–911.

Ha, M., and Kim, V.N. (2014). Regulation of microRNA biogenesis. Nat. Rev. Mol. Cell Biol. *15*, 509–524.

Han, J., Lee, Y., Yeom, K.H., Kim, Y.K., Jin, H., and Kim, V.N. (2004). The Drosha-DGCR8 complex in primary microRNA processing. Genes Dev. *18*, 3016–3027.

Heale, B.S., Keegan, L.P., McGurk, L., Michlewski, G., Brindle, J., Stanton, C.M., Caceres, J.F., and O'Connell, M.A. (2009). Editing independent effects of ADARs on the miRNA/siRNA pathways. EMBO J. *28*, 3145–3156.

Heo, I., Ha, M., Lim, J., Yoon, M.J., Park, J.E., Kwon, S.C., Chang, H., and Kim, V.N. (2012). Mono-uridylation of pre-microRNA as a key step in the biogenesis of group II let-7 microRNAs. Cell *151*, 521–532.

Hutvágner, G., McLachlan, J., Pasquinelli, A.E., Bálint, E., Tuschl, T., and Zamore, P.D. (2001). A cellular function for the RNA-interference enzyme Dicer in the maturation of the let-7 small temporal RNA. Science *293*, 834–838.

Kelley, L.A., and Sternberg, M.J. (2009). Protein structure prediction on the Web: a case study using the Phyre server. Nat. Protoc. *4*, 363–371.

Kim, V.N., Han, J., and Siomi, M.C. (2009). Biogenesis of small RNAs in animals. Nat. Rev. Mol. Cell Biol. *10*, 126–139.

Kim, Y., Yeo, J., Lee, J.H., Cho, J., Seo, D., Kim, J.S., and Kim, V.N. (2014). Deletion of human tarbp2 reveals cellular microRNA targets and cell-cycle function of TRBP. Cell Rep. *9*, 1061–1074.

Kim, Y.K., Kim, B., and Kim, V.N. (2016). Re-evaluation of the roles of DROSHA, Export in 5, and DICER in microRNA biogenesis. Proc. Natl. Acad. Sci. USA *113*, E1881–E1889.

Kimanius, D., Forsberg, B.O., Scheres, S.H., and Lindahl, E. (2016). Accelerated cryo-EM structure determination with parallelisation using GPUs in RELION-2. Elife *5*, e18722.

Kowalinski, E., Lunardi, T., McCarthy, A.A., Louber, J., Brunel, J., Grigorov, B., Gerlier, D., and Cusack, S. (2011). Structural basis for the activation of innate immune pattern-recognition receptor RIG-I by viral RNA. Cell *147*, 423–435.

Kozomara, A., and Griffiths-Jones, S. (2014). miRBase: annotating high confidence microRNAs using deep sequencing data. Nucleic Acids Res. *42*, D68–D73.

Kucukelbir, A., Sigworth, F.J., and Tagare, H.D. (2014). Quantifying the local resolution of cryo-EM density maps. Nat. Methods *11*, 63–65.

Kurzynska-Kokorniak, A., Pokornowska, M., Koralewska, N., Hoffmann, W., Bienkowska-Szewczyk, K., and Figlerowicz, M. (2016). Revealing a new activity of the human Dicer DUF283 domain in vitro. Sci. Rep. *6*, 23989.

Kwon, S.C., Nguyen, T.A., Choi, Y.G., Jo, M.H., Hohng, S., Kim, V.N., and Woo, J.S. (2016). Structure of Human DROSHA. Cell *164*, 81–90.

Lau, P.W., Potter, C.S., Carragher, B., and MacRae, I.J. (2009). Structure of the human Dicer-TRBP complex by electron microscopy. Structure *17*, 1326–1332.

Lau, P.W., Guiley, K.Z., De, N., Potter, C.S., Carragher, B., and MacRae, I.J. (2012). The molecular architecture of human Dicer. Nat. Struct. Mol. Biol. *19*, 436–440.

Lee, H.Y., and Doudna, J.A. (2012). TRBP alters human precursor microRNA processing in vitro. RNA *18*, 2012–2019.

Lee, Y., Jeon, K., Lee, J.T., Kim, S., and Kim, V.N. (2002). MicroRNA maturation: stepwise processing and subcellular localization. EMBO J. *21*, 4663–4670.

Lee, Y., Ahn, C., Han, J., Choi, H., Kim, J., Yim, J., Lee, J., Provost, P., Rådmark, O., Kim, S., and Kim, V.N. (2003). The nuclear RNase III Drosha initiates microRNA processing. Nature *425*, 415–419.

Lee, Y., Hur, I., Park, S.Y., Kim, Y.K., Suh, M.R., and Kim, V.N. (2006). The role of PACT in the RNA silencing pathway. EMBO J. *25*, 522–532.

Li, X., Mooney, P., Zheng, S., Booth, C.R., Braunfeld, M.B., Gubbens, S., Agard, D.A., and Cheng, Y. (2013). Electron counting and beam-induced motion correction enable near-atomic-resolution single-particle cryo-EM. Nat. Methods *10*, 584–590.

Li, X., Zheng, S., Agard, D.A., and Cheng, Y. (2015). Asynchronous data acquisition and on-the-fly analysis of dose fractionated cryoEM images by UCSFImage. J. Struct. Biol. *192*, 174–178.

Lin, Y.C., Boone, M., Meuris, L., Lemmens, I., Van Roy, N., Soete, A., Reumers, J., Moisse, M., Plaisance, S., Drmanac, R., et al. (2014). Genome dynamics of the human embryonic kidney 293 lineage in response to cell biology manipulations. Nat. Commun. *5*, 4767.

Ma, E., MacRae, I.J., Kirsch, J.F., and Doudna, J.A. (2008). Autoinhibition of human dicer by its internal helicase domain. J. Mol. Biol. *380*, 237–243.

Macrae, I.J., Zhou, K., Li, F., Repic, A., Brooks, A.N., Cande, W.Z., Adams, P.D., and Doudna, J.A. (2006). Structural basis for double-stranded RNA processing by Dicer. Science *311*, 195–198.

Matsuda, T., and Cepko, C.L. (2004). Electroporation and RNA interference in the rodent retina in vivo and in vitro. Proc. Natl. Acad. Sci. USA *101*, 16–22.

Mindell, J.A., and Grigorieff, N. (2003). Accurate determination of local defocus and specimen tilt in electron microscopy. J. Struct. Biol. *142*, 334–347.

Nicholson, A.W. (2014). Ribonuclease III mechanisms of double-stranded RNA cleavage. Wiley Interdiscip. Rev. RNA *5*, 31–48.

Noland, C.L., Ma, E., and Doudna, J.A. (2011). siRNA repositioning for guide strand selection by human Dicer complexes. Mol. Cell *43*, 110–121.

Ota, H., Sakurai, M., Gupta, R., Valente, L., Wulff, B.E., Ariyoshi, K., Iizasa, H., Davuluri, R.V., and Nishikura, K. (2013). ADAR1 forms a complex with Dicer to promote microRNA processing and RNA-induced gene silencing. Cell *153*, 575–589.

Park, J.E., Heo, I., Tian, Y., Simanshu, D.K., Chang, H., Jee, D., Patel, D.J., and Kim, V.N. (2011). Dicer recognizes the 5′ end of RNA for efficient and accurate processing. Nature *475*, 201–205.

Pettersen, E.F., Goddard, T.D., Huang, C.C., Couch, G.S., Greenblatt, D.M., Meng, E.C., and Ferrin, T.E. (2004). UCSF Chimera–a visualization system for exploratory research and analysis. J. Comput. Chem. *25*, 1605–1612.

Purzycka, K.J., Popenda, M., Szachniuk, M., Antczak, M., Lukasiak, P., Blazewicz, J., and Adamiak, R.W. (2015). Automated 3D RNA structure prediction using the RNAComposer method for riboswitches. Methods Enzymol. *553*, 3–34.

Qin, H., Chen, F., Huan, X., Machida, S., Song, J., and Yuan, Y.A. (2010). Structure of the Arabidopsis thaliana DCL4 DUF283 domain reveals a noncanonical double-stranded RNA-binding fold for protein-protein interaction. RNA *16*, 474–481.

Rohou, A., and Grigorieff, N. (2015). CTFFIND4: Fast and accurate defocus estimation from electron micrographs. J. Struct. Biol. *192*, 216–221.

Scheres, S.H. (2012). RELION: implementation of a Bayesian approach to cryo-EM structure determination. J. Struct. Biol. *180*, 519–530.

Schneider, C.A., Rasband, W.S., and Eliceiri, K.W. (2012). NIH Image to ImageJ: 25 years of image analysis. Nature Methods *9*, 671–675.

Spitale, R.C., Flynn, R.A., Zhang, Q.C., Crisalli, P., Lee, B., Jung, J.W., Kuchelmeister, H.Y., Batista, P.J., Torre, E.A., Kool, E.T., et al. (2015). Structural imprints in vivo decode RNA regulatory mechanisms. Nature *519*, 486–490.

Starega-Roslan, J., Koscianska, E., Kozlowski, P., and Krzyzosiak, W.J. (2011). The role of the precursor structure in the biogenesis of microRNA. Cell. Mol. Life Sci. *68*, 2859–2871.

Takeshita, D., Zenno, S., Lee, W.C., Nagata, K., Saigo, K., and Tanokura, M. (2007). Homodimeric structure and double-stranded RNA cleavage activity of the C-terminal RNase III domain of human dicer. J. Mol. Biol. *374*, 106–120.

Tang, G., Peng, L., Baldwin, P.R., Mann, D.S., Jiang, W., Rees, I., and Ludtke, S.J. (2007). EMAN2: an extensible image processing suite for electron microscopy. J. Struct. Biol. *157*, 38–46.

Taylor, D.W., Ma, E., Shigematsu, H., Cianfrocco, M.A., Noland, C.L., Nagayama, K., Nogales, E., Doudna, J.A., and Wang, H.W. (2013). Substrate-specific structural rearrangements of human Dicer. Nat. Struct. Mol. Biol. *20*, 662–670.

Tian, Y., Simanshu, D.K., Ma, J.B., Park, J.E., Heo, I., Kim, V.N., and Patel, D.J. (2014). A phosphate-binding pocket within the platform-PAZ-connector helix cassette of human Dicer. Mol. Cell *53*, 606–616.

Tsutsumi, A., Kawamata, T., Izumi, N., Seitz, H., and Tomari, Y. (2011). Recognition of the pre-miRNA structure by Drosophila Dicer-1. Nat. Struct. Mol. Biol. *18*, 1153–1158.

Wang, H.W., Noland, C., Siridechadilok, B., Taylor, D.W., Ma, E., Felderer, K., Doudna, J.A., and Nogales, E. (2009). Structural insights into RNA processing by the human RISC-loading complex. Nat. Struct. Mol. Biol. *16*, 1148–1153.

Wilson, R.C., Tambe, A., Kidwell, M.A., Noland, C.L., Schneider, C.P., and Doudna, J.A. (2015). Dicer-TRBP complex formation ensures accurate mammalian microRNA biogenesis. Mol. Cell *57*, 397–407.

Wu, B., Peisley, A., Richards, C., Yao, H., Zeng, X., Lin, C., Chu, F., Walz, T., and Hur, S. (2013). Structural basis for dsRNA recognition, filament formation, and antiviral signal activation by MDA5. Cell *152*, 276–289.

Zheng, S.Q., Palovcak, E., Armache, J.P., Verba, K.A., Cheng, Y., and Agard, D.A. (2017). MotionCor2: anisotropic correction of beam-induced motion for improved cryo-electron microscopy. Nat. Methods *14*, 331–332.

Zou, J., Chang, M., Nie, P., and Secombes, C.J. (2009). Origin and evolution of the RIG-I like RNA helicase gene family. BMC Evol. Biol. *9*, 85.

STAR★METHODS

KEY RESOURCES TABLE

REAGENT or RESOURCE	SOURCE	IDENTIFIER
Chemicals, Peptides, and Recombinant Proteins		
SMM 293-TI	Sino Biological Inc.	Cat# M293TI
Polyethylenimines	Polysciences	Cat# 23966-2
d-Desthiobiotin	Sigma	Cat# 2-1201
Protease Inhibitor Cocktail Tablets	Roche	Cat# 04693159001
Phenylmethyl sulfonyl fluoride	AMRESCO	Cat# 0754
Critical Commercial Assays		
Strep-Tactin @Sepharose	IBA Life Science	Cat# 2-1201
Superose 6 Increase 5/150 GL	GE Healthcare	Cat# 29-0915-97
Deposited Data		
icSHAPE	this paper	GEO: GSE110516
Coordinates of hDicer-TRBP	this paper	PDB: 5ZAK
Cryo-EM map of hDicer-TRBP	this paper	EMDB: 6904
Coordinates of HDicer-TRBP-pre-let-7 (class I)	this paper	PDB: 5ZAL
Cryo-EM map of hDicer-TRBP-pre-let-7 (class I)	this paper	EMDB: 6905
Coordinates of hDicer-TRBP-pre-let-7 (class II)	this paper	PDB: 5ZAM
Cryo-EM map of hDicer-TRBP-pre-let-7 (class II)	this paper	EMDB: 6906
Coordinates of human MDA5 bound with dsRNA	Wu et al., 2013	PDB: 4GL2
Coordinates of *Arabidopsis thaliana* DCL4 DUF283	Qin et al., 2010	PDB: 2KOU
Coordinates of human DROSHA in complex with the C-terminal tail of DGCR8	Kwon et al., 2016	PDB: 5B16
Coordinates of RNase IIIb and dsRBD of mouse Dicer	Du et al., 2008	PDB: 3C4T
Coordinates of the human Dicer-TRBP interface	Wilson et al., 2015	PDB: 4WYQ
Coordinates of human Dicer Platform-PAZ-Connector Helix cassette bound with 12-mer siRNA	Tian et al., 2014	PDB: 4NGD
Coordinates of human Dicer Platform-PAZ-Connector Helix cassette bound with 16-mer dsRNA	Tian et al., 2014	PDB: 4NHA
Coordinates of duck RIG-I bound with 19-mer dsRNA	Kowalinski et al., 2011	PDB: 4A36
Coordinates of duck RIG-I helicase domain	Kowalinski et al., 2011	PDB: 4A2P
Coordinates of *Aquifex aeolicus* RNase III (D44N) complexed with dsRNA	Gan et al., 2006	PDB: 2EZ6
Coordinates of Giardia Dicer	Macrae et al., 2006	PDB: 2FFL
Coordinates of duck RIG-I helicase domain	Kowalinski et al., 2011	PDB: 4A2P
Experimental Models: Cell Lines		
FreeStyle 293-F Cells	ThermoFisher	Cat# R79007
Oligonucleotides		
Strep tagged hDicer forward primer: 5′-GGGGTACCATGAAAAGCCCTGCTTTG-3′	this paper	N/A
Strep tagged hDicer reverse primer: 5′-CCGCTCGAGCGGTCAGCTATTGGGAACCTG-3′	this paper	N/A
Vsv tagged hDicer forward primer: 5′-CGAATTCGCGGCCGCTATGAAAAGCCCTGCTTTGCAACC-3′	this paper	N/A
Vsv tagged hDicer reverse primer: 5′-GCAAGCTTCTCGAGTCAGCTATTGGGAACCTGAG-3′	this paper	N/A

(*Continued on next page*)

Continued

REAGENT or RESOURCE	SOURCE	IDENTIFIER
TRBP forward primer: 5′- CGACGCGTATGAGTGAAGAGGAGCAAGG-3′	this paper	N/A
Strep tagged TRBP reverse primer: 5′- AAGGAAAAAAGCGGCCGCAAAAGGAA AATCACTTGCTGCCTGCCATGATCTTGAGG	this paper	N/A
Primers for truncated hDicer constructs, see Table S2	this paper	N/A
The pre-let-7 RNA (5′- UGAGGUAGUAGGUUGUAUAGUUUUAGGGU CACACCCACCACUGGGAGA UAACUAUACAACUCUACUGUCUUACC-3′	this paper	N/A
Recombinant DNA		
pCAG-5′vsv-hDicer	this paper	N/A
pCAG-3′strep-TRBP	this paper	N/A
pCAG-5′strep-hDicerΔHEL2i	this paper	N/A
pCAG-5′strep-hDicerΔHEL2+2i,	this paper	N/A
pCAG-5′strep-hDicerΔDExD/H-box helicase	this paper	N/A
Software and Algorithms		
UCSFImage4	Li et al., 2015	http://cryoem.ucsf.edu/software/UCSFimage.html
AutoEMation	written by Dr. Jianlin Lei	jllei@tsinghua.edu.cn
Motioncorr	Li et al., 2013	http://cryoem.ucsf.edu/software/driftcorr.html
MotionCor2	Zheng et al., 2017	http://msg.ucsf.edu/em/software/motioncor2.html
RELION2.0	Kimanius et al., 2016	http://www2.mrc-lmb.cam.ac.uk/relion
ResMap	Kucukelbir et al., 2014	http://resmap.sourceforge.net
CHIMERA	Pettersen et al., 2004	http://www.cgl.ucsf.edu/chimera
PHENIX	Adams et al., 2010	https://www.phenix-online.org
PyMOL	Schrodinger LLC	http://www.pymol.org
COOT	Emsley and Cowtan, 2004	https://www2.mrc-lmb.cam.ac.uk/personal/pemsley/coot
CTFFIND4	Rohou and Grigorieff, 2015	http://grigoriefflab.janelia.org/ctffind4
GraphPad Prism	GraphPad Software	https://www.graphpad.com/scientific-software/prism/
ImageJ 1.50i	Schneider et al., 2012	https://imagej.nih.gov/ij/
Other		
R1.2/1.3 400 mesh Au holey carbon grids	Quantifoil	Cat#1210627

CONTACT FOR REAGENT AND RESOURCE SHARING

Further information and requests for resources and reagents should be directed to and will be fulfilled by the Lead Contact, Hong-Wei Wang (hongweiwang@tsinghua.edu.cn).

EXPERIMENTAL MODEL AND SUBJECT DETAILS

Cell culture

The FreeStyle 293-F cell line (ThermoFisher) is derived from the 293 cell line (HEK293) which is a permanent line established from normal human embryonic kidney cells transformed with sheared human adenovirus type 5DNA (Graham et al., 1977). HEK293 cells have a complex karyotype that contains multiple X chromosomes and lack of any trace of Y chromosome derived sequence, which suggests that the source fetus was female(Lin et al., 2014)). The expressed adenovirus E1A protein joins in transactivation of some viral promoters to increase the expression levels of proteins. The FreeStyle 293-F cell line is a variant of the 293 cell line that has been

adapted to suspension growth in serum free medium, in this project, FreeStyle 293-F cell line were cultured in SMM 293-TI medium (Sino Biological Inc.) at 37°C with 8% CO2 and shaking at 120 rpm.

METHOD DETAILS

Recombinant construct preparation and protein expression

In order to purify the apo-hDicer, hDicer was fused into a plasmid with 2x-Strep tag. Primers containing KpnI and Xho I restriction enzymes were used to amplify the coding region from the recombinant pFastBac-hDicer plasmid (kindly gifted by the Doudna Lab) (forward primer: 5′-GGGGTACCATGAAAAGCCCTGCTTTG-3′, reverse primer: 5′-CCGCTCGAGCGGTCAGCTATTG GGAACCTG-3′). For the hDicer-TRBP complex, hDicer and TRBP were fused to Vsv-G-tag and 2x-Strep tag, respectively. To construct the vectors expressing Vsv-G-tagged hDicer protein and 2x-Strep-tagged TRBP, templates prepared from recombinant pFastBac-hDicer plasmid and pet28-MBP-TRBP plasmid (kindly gifted by the Doudna Lab) were used to amplify the coding region of hDicer and human TRBP, respectively (hDicer forward primer: 5′-CGAATTCGCGGCCGCTATGAAAAGCCCTGCTTTGCAACC-3′, hDicer reverse primer: 5′-GCAAGCTTCTCGAGTCAGCTATTGGGAACCTGAG-3′, TRBP forward primers: 5′- CGACGCGTATGAG TGAAGAGGAGCAAGG-3′, TRBP reverse primers: 5′- AAGGAAAAAAGCGGCCGCAAAAGGAAAATCACTTGCTGCCTGCCATGATC TTGAGG). Xho I and Not I were used to cleave the amplified Vsv-G-hDicer products. Mlu I and Not I were used to cleave the amplified TRBP products. All the cleaved fragments were subsequently inserted into the pCAG vector (Matsuda and Cepko, 2004). For the constructs expressing ΔHEL2i, ΔHEL2+2i and ΔDExD/H-box helicase hDicer protein, Q5 Site-Directed Mutagenesis Kit (NEB Inc.) were used to delete the HEL2i, HEL2+2i and DExD/H-box helicase based on the 2x-Strep-tagged hDicer vector. For the expression of apo-hDicer, hDicer-TRBP complex and fragment truncated hDicer, HEK293F cells (Sino Biological Inc.) were grown in suspension culture (SMM293T-I medium from Sino Biological Inc.) at 37°C under 8% CO_2. When the cell density reached 1.5 × 10^6 cells per ml, the pCAG-Vsv-G-hDicer vector and pCAG-2x-Strep-TRBP vector were co-transfected into cells with a ratio of 1:2. For one liter of cell culture, 1.0 mg of plasmid and 2.0 mg PEI (25-kDa linear polyethylenimines, Polysciences) were each added to a 20 ml fresh cell culture medium solution and incubated for 10-15 min separately at room temperature. The plasmid and PEI solution were then mixed together and incubated for another 15-30 min at room temperature before transfection. Transfected cells were cultured in suspension for 48 hr before harvesting. This procedure was also used to express the 2x-Strep-tagged hDicer and truncated hDicer proteins.

Purification of Strep-tagged proteins

Cells transfected with the pCAG vector expressing human Dicer and TRBP were pelleted at 700 g. The cells were then re-suspended with ice cooled lysis buffer containing 100 mM Tris-HCl (pH 8.0), 150 mM NaCl, 1% Triton X-100, 1 mM DTT, 1 mM PMSF, 2 mM EDTA and protease inhibitor cocktails (Roche). The suspended cells were placed at 4°C and shaken gently for 20 min. The suspension was centrifuged at 30,000 rpm (Ti 75 rotor, Beckman Coulter, Inc) for 1 hr. The supernatant was filtered through a 0.22 μm filter (Millipore) and loaded onto a column packed with 1 mL Strep-Tactin @Sepharose (IBA Life Science). The column was washed with 100 mL of washing buffer containing 100 mM Tris-HCl (pH 8.0), 300 mM NaCl, 1 mM DTT, 2 mM EDTA and 1 mM PMSF. The human Dicer-TRBP complex were then eluted with 5 mL elution buffer containing 100 mM Tris-HCl (pH 8.0), 150 mM NaCl, 1 mM DTT, 2 mM EDTA and 2.5 mM desthiobiotin (Sigma-Aldrich). Protein solutions were pooled together and concentrated to 4 mg/ml for storage with a 100 kDa cut-off Centricon (Millipore). The concentrated solution was subjected to size exclusion column (Superose™ 6 Increase 5/150 GL, GE Healthcare) equilibrated with gel filtration buffer containing 50 mM Tris-HCl (pH 8.0), 100 mM NaCl, 1 mM DTT, 2 mM EDTA. All the above operations were executed in a 4°C cold room. The very similar method was also applied to purify the 2x-Strep-tagged hDicer and truncated hDicer proteins.

In vitro reconstitution of the hDicer-TRBP-pre-let-7 complex

The pre-let-7 RNA (5′- UGAGGUAGUAGGUUGUAUAGUUUUAGGGUCACACCCACCACUGGGAGAUAACUAUACAAUCUACUG UCUUACC-3′) was synthesized by Genescript Inc. In order to form the hairpin pre-let-7, we heated the RNA at 90°C for 3 min then snap-cooled it on ice for 5 min. The purity and homogeneity of the RNA was verified by native and denature gel electrophoresis before all experiments. In order to reconstitute the hDicer-TRBP-pre-let-7 complex, we mixed ∼200 μg (0.8 nmol) hDicer-TRBP complex and ∼54 μg (2.3 nmol) pre-let-7 RNA in 50 μl of gel filtration buffer containing 2 mM Ca^{2+} and incubated the mixture on ice for 40 min. After this, the mixture was applied to a Superose 6 Increase 5/150 GL (GE Healthcare) column installed on an ÄKTAmicro (GE Healthcare) equilibrated in gel filtration buffer containing 2 mM Ca^{2+}. Fractions containing the hDicer-TRBP-pre-let-7 complex were collected at a final concentration of ∼0.4 mg/ml.

Dicing-activity assay

The modified pre-let-7 RNA (5′-6-FAM-UGAGGUAGUAGGUUGUAUAGUUUUAGGGUCACAC CCACCACUGGGAGAUAACUAU ACAAUCUACUGUCUUACC-3′, RNA was synthesized by Genescript Inc.) was used in dicing assay. All proteins were replaced with the reaction buffer containing 30 mM Tris-HCl (pH 6.8), 50 mM NaCl, 2 mM MgCl2, 0.1% Triton X-100, 15 ± 25% glycerol and 1 mM DTT through a desalting column just before the dicing activity assays. We mixed 2 μl of 20 nM FAM labeled pre-let-7 with 2 μl of 100 nM hDicer in a final 15 μl reaction solution and incubated the solution at 37°C with a time course as mentioned in

the maintext. The reaction was stopped with RNA loading buffer containing 8 M Urea, 1 x TBE, 0.05% Bromphenol blue and 0.05% Xylene cyanol, boiled for 4 min, and subsequently chilled on ice. RNA products were analyzed on 18% polyacrylamide, 8 M urea denaturing gel electrophoresis, and visualized with a Typhoon Trio Imager (Amersham Biosciences).

Electrophoretic mobility shift assay (EMSA)

For EMSA, pre-let-7 labeled with FAM at the 5′ terminus was incubated with different hDicer constructs on ice for 40 min in a 20 μl volume containing 30 mM Tris-HCl (pH 6.8), 25 mM NaCl, 2 mM MgCl2, 1 mM DTT and 2 mM EDTA. Mutant Dicer was added with increasing concentrations of 0, 15, 35, 65, 125, 250, 500, 1000, 2000 nM in lanes 1-9. And each lane contained an approximately 100 pM 5′ FAM-labeled pre-let-7. Samples were resolved through 6% native acrylamide gels in 0.5 × Tris-glycine buffer under an electric field of 15 V/cm for 70 min and the gels were subsequently visualized with a Typhoon Trio Imager (Amersham Biosciences).

RNA-probing assay and RNase limited-digestion assay

RNA probing assay was performed as previously described (Spitale et al., 2015). Briefly, free pre-let-7 was prepared as in the cryo-EM studies and dicing assays. To study the conformational effect of proteins on pre-let-7, hDicer-TRBP were pre-incubated with pre-let-7 on ice for 30 min. For the RNA probing, chemical NAI-N3 was added to the sample to a final concentration 100 mM, mixed gently, and incubated at 37°C for 10 min. 35 μl of buffer RLT was added to stop the reaction on ice. The RNA was purified with an RNeasy mini column and eluted with 50 μl of pure water twice (100 μl final volume). The modified RNA was captured with DIBO-biotin at 37°C for 2 hr incubation and then purified with the Zymo RNA kit. It was then subjected to end repair, linker ligation and reverse transcription. Transcribed cDNA was enriched by biotin together with the RNA moiety. cDNA libraries were amplified using qPCR with about 13-15 cycles. The library was then sequenced using Illumina X-ten pair-end 150 sequencing. Only the left reads were used for the analysis. After removing duplicated reads and trimming of PCR primers, reads longer than 25nt were kept for further analysis. The next pipeline is done using the icSHAPE protocol (Flynn et al., 2016).

All RNase digestion assay were performed in solutions without Mg^{2+} except special indication. RNase cleavage reactions were performed with buffer containing 350 nM NaCl, 50 mM Tris-HCl (pH 8.0), 1 mM DTT at 37°C for 2 min. pre-let-7 (40 nM), hDicer-TRBP (1 mg/ml), RNase A (0.1 μg/ml), BSA (1 mg/ml) were added in the reaction with indicated volumes on top of each lane. Pre-let-7 labeled with FAM at the 5′ terminus was used in the RNase digestion assay.

Cryo-EM specimen preparation and data acquisition

The purified hDicer-TRBP or hDicer-TRBP-pre-let-7 complex was diluted to a concentration of about 2 μM in a buffer containing 50 mM Tris, pH 8.0, 150 mM NaCl, 1 mM DTT (and additional 2 mM $CaCl_2$ for hDicer-TRBP-pre-let-7 complex) immediately before preparing the frozen-hydrated grids. We found the following grid preparation conditions critical to make good frozen-hydrated grids of hDicer-TRBP and hDicer-TRBP-pre-let-7 complexes. We first evaporated a layer of 40 nm thick gold foil over a gold Quantifoil holey carbon grid (R1.2/1.3) using a gold sputter (HITACHI) and then removed the carbon film on the back of the grid in a plasma-cleaning instrument (TED PELLA INC.) for 10 min. The grid treated as above was glow-discharged immediately before making the cryo-EM specimen. In an FEI Vitrobot Mark VI, we placed 4 μl of the protein or protein-RNA complexes onto the grid, blotted the grid 3.0 s in 100% humidity at 22°C, and plunged the grid in liquid ethane cooled by liquid nitrogen. For hDicer-TRBP sample, the frozen-dehydrated grid was transferred to a Titan Krios electron microscope equipped with a Gatan K2 Summit direct-electron counting camera for examination and data acquisition. The microscope was operated at 300 kV, and images of the specimen were recorded with a defocus range of −2.5 to −3.5 μm in super resolution mode of the K2 camera, yielding a pixel size of 0.653 Å. A total of 7,581 32-frame movie stacks of the Dicer-TRBP complex were recorded using the semi-automated low-dose acquisition program UCSF-Image4 (Li et al., 2015), with an electron dose rate of 6.25 electrons per $Å^2$ per second and total exposure time of 8 s. Thus, the total accumulated dose on the specimen was about 50 electrons per $Å^2$ and each frame had an exposure time of 0.25 s. The hDicer-TRBP-pre-let-7 data were collected on a Titan Krios electron microscope operated at 300ckV equipped with a Cs-corrector and a Gatan K2 Summit direct electron detection camera (Gatan) using AutoEMation. We collected 2,849 32-frame movie stacks in super-resolution mode with a pixel size of 0.685cÅ across a defocus range of −2.5 to −3.5cμm. The total dose also 50 $e^-/Å^2$, was attained by using 5.44cs exposure time.

Image processing of electron micrographs

For each movie stack, the 32 frames collected from the K2 Summit camera were decimated twice, aligned and summed together using the frame-based motion correction algorithm to generate a motion-corrected micrograph stack for further image processing using the MotionCorr software (Li et al., 2013). The motion-corrected stacks were future aligned and dose-weighted by MotionCor2 (Zheng et al., 2017). The contrast-transfer function (CTF) parameters of each micrograph were determined using CTFFIND4 (Mindell and Grigorieff, 2003). Approximately 10,000 particles of each dataset were semi-automatically picked using EMAN2 from ~50 micrographs (Tang et al., 2007) and subjected to reference-free 2D-classification in RELION (Scheres, 2012). The best representative 2D class averages were selected as templates for automatic particle picking of all the micrographs in RELION. The whole set of particles were cleaned to remove ice contaminants or junk particles by one round of 2D classification and one round of reference-based 3D-classification using an initial 3D model from our previous reconstruction of hDicer (EMD-5601), low-pass filtered to 60 Å. Both of the two datasets, only one class showed structural features of higher detail after the 3D-classification and particles in

this class was selected for 3D auto-refinement separately. For the hDicer-TRBP dataset, we did further 3D-classification and two minuscule different maps were reconstructed. For the hDicer-TRBP-pre-let7 dataset, we focused on the more flexible pre-let7 loop region and did further 3D classification by applying a local mask. We did not perform image alignment during this step. Finally, two obvious different conformational reconstructions were generated after 3D auto-refinement and post-processing in RELION. More details related to data processing are summarized in Table S1.

Model building of the cryo-EM maps

We first used Phyre online server to get the initial model of hDicer (Kelley and Sternberg, 2009). Phyre took the sequence information provided by the user to search the whole Protein Data Bank for homologous structure and generated several models based on different PDBs. Phyre also provided the confidence values of the models. Confidence value represented the homologous degree between target sequence and reference. For residues 44-593, almost all the models given by Phyre were similar and we chose the highest confidence one (confidence: 100) that was based on the structure of MDA5 (PDB: 4GL2). For residues 624-726, we chose the best fitted 2KOU as reference, the corresponding confidence value was also 100. For residues 1286-1620, Phyre gave only one model based on the Drosha structure (PDB: 5B16). For residues 1653-1912, we chose the RNase IIIb of mouse dicer (PDB: 3C4T) with 96% of common sequence to hDicer as the template. We used a rigid-body fitting to dock the dsRBD domain into the low-passed filtered 3D map, in which a prominent extra density attached to the RNase IIIb domain exists. For residues 266-387 (PDB: 4WYQ) and 764-1073 (PDB: 4NGD), the available crystal structures were directly used. We docked all the atomic models of separated domains in our EM map in UCSF-Chimera (Pettersen et al., 2004) and merged all the coordinates into one PDB file in Coot (Emsley and Cowtan, 2004). 1,314 residues were modeled in a final hDicer, accounting for about 70% of the molecule. The atomic model of TRBP residues 289-263 were taken from PDB 4WYQ. A final merged atomic model was further refined against the Dicer-TRBP 3D map with stereochemical and secondary structure restraints using phenix.real_space_refine in the Phenix software (Adams et al., 2010). For the Dicer-TRBP-pre-let-7 complex, the 3D model of pre-let-7 RNA was obtained using an online RNA 3D structural prediction server RNAcomposer (Purzycka et al., 2015). We docked the atomic models of Dicer-TRBP and pre-let-7 separately in the 3D maps of hDicer-TRBP-pre-let-7 complex in UCSF-Chimera. Before the final model refinement in real space using Phenix, only the well fitted regions in the RNA models were kept.

Quantification and Statistical Analysis

For the quantification of the impact of HEL2i, HEL2+2i and DExD/H-box helicase domain on dicing activity (Figures 6B and S7A), measurements were carried out using the ImageJ. GraphPad Prism was used to perform the statistical analysis of measuring results. Each data point represents the average of three independent experiments. Error bars represent SD.

DATA AND SOFTWARE AVAILABILITY

Data resources

The accession numbers of the 4.4 Å resolution EM map of hDicer-TRBP complex, the 4.7 Å resolution EM map of hDicer-TRBP-pre-let-7 class I complex and the 5.7 Å resolution EM map of hDicer-TRBP-pre-let-7 class II complex and their corresponding coordinates reported in this paper are EMDB: 6904, 6905, and 6906,and PDB: 5ZAK, 5ZAL, 5ZAM, respectively.

The accession codes of the icSHAPE data are GSE110516.

Cell

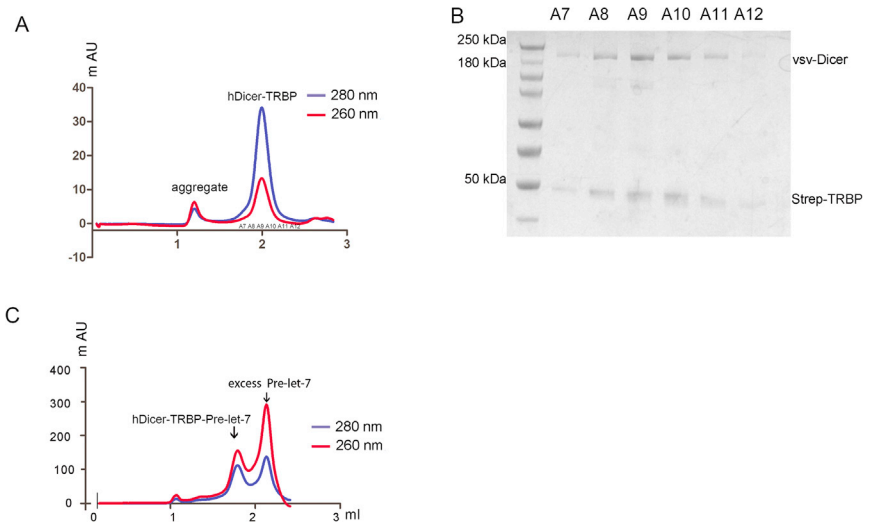

Figure S1. Purification and Reconstitution of hDicer-TRBP and hDicer-TRBP-Pre-let-7 Complexes, Related to Figure 1

(A) Size-exclusion chromatography of the hDicer-TRBP complex.

(B) SDS-PAGE of the protein fractions from the size-exclusion chromatography.

(C) Size-exclusion chromatography of in vitro reconstituted hDicer-TRBP-pre-let-7 complex.

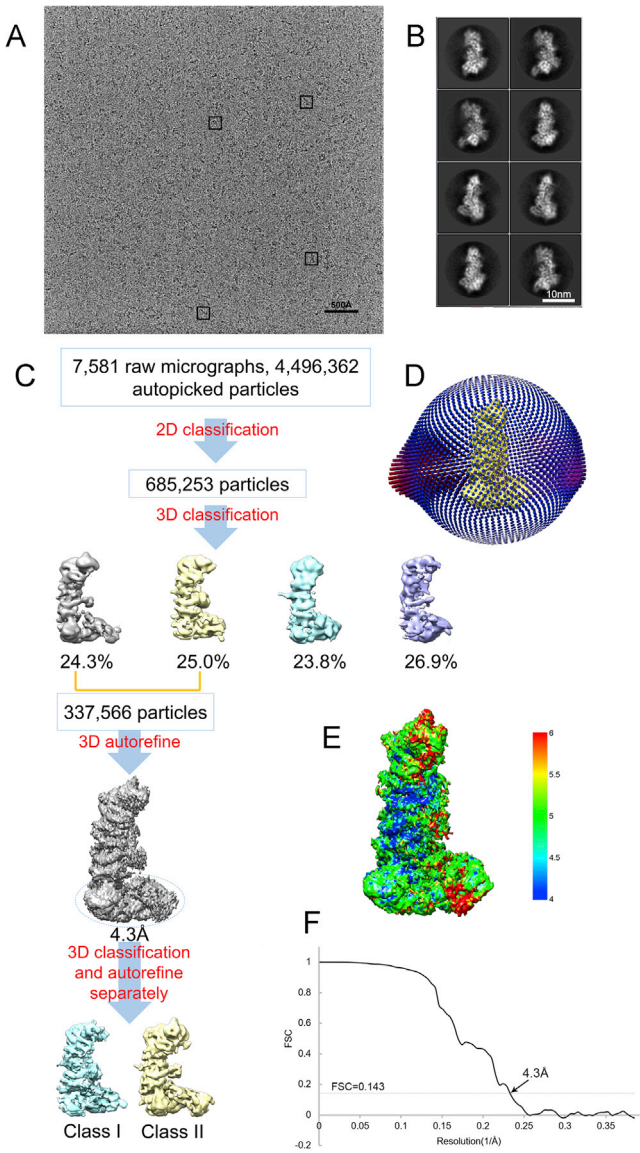

Figure S2. Flowchart of Cryo-EM Reconstruction of the hDicer-TRBP Complex, Related to Figure 1

(A) A representative area from a raw micrograph of the frozen-hydrated hDicer-TRBP complex taken from the 300 kV Titan Krios microscope. Several typical particles are marked by square boxes.

(B) Typical 2D class averages of the complex.

(C) Schematic outline of the image processing steps used to obtain the 4.3 Å resolution cryo-EM reconstruction of the hDicer-TRBP complex. Local classification of the final 3D reconstruction that mainly focused on the DExD/H-box helicase domain yielded two maps showing variation mainly in the helicase domain.

(D) Angular distribution of particles for the final 3D reconstruction.

(E) Local resolution map of the final 3D reconstruction estimated using RESMAP.

(F) Corrected Fourier Shell Correlation (FSC) curve of the final 3D reconstruction of hDicer-TRBP complex after post-processing in RELION.

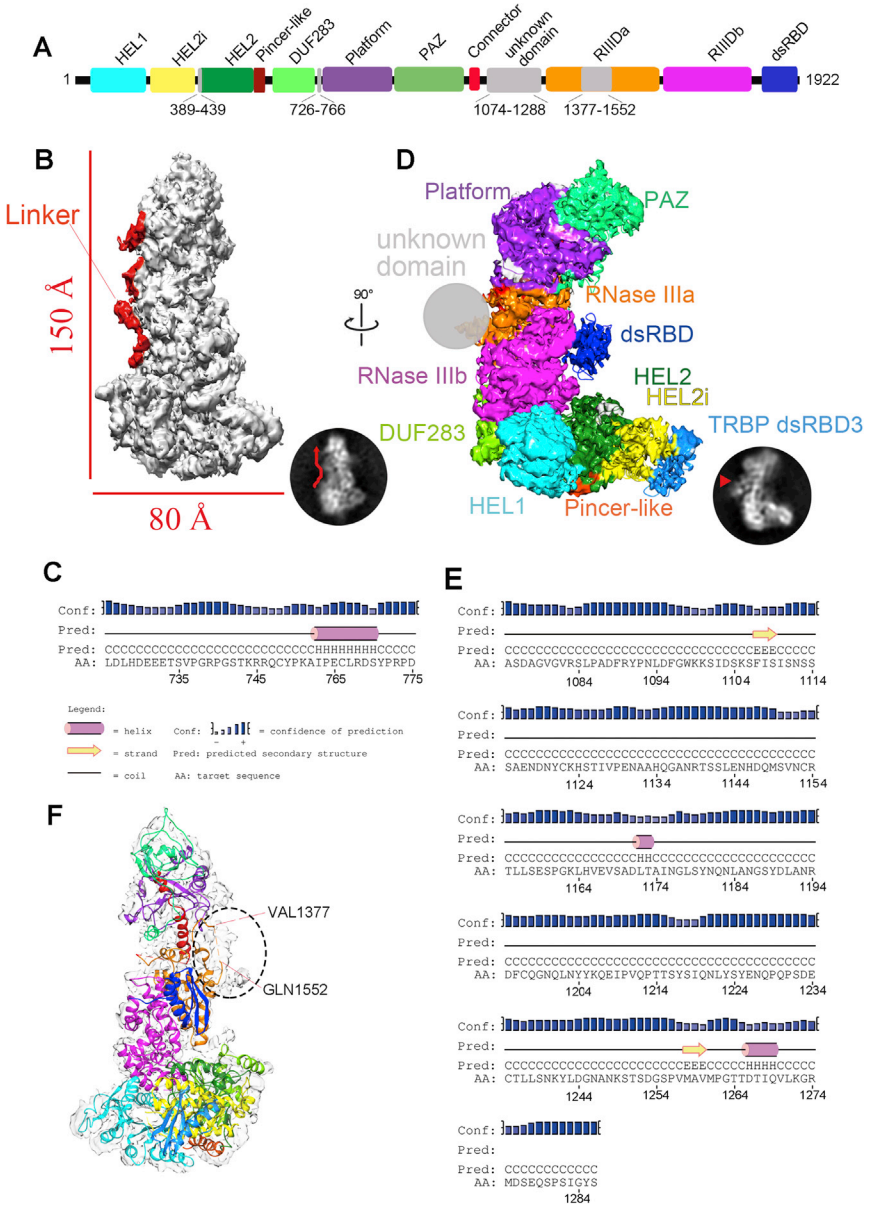

Figure S3. Analysis of the Less Ordered Linker and Unknown Domain, Related to Figure 1

(A) Schematic domain distribution of full-length human Dicer. The residues that were not built for their atomic models are labeled in gray color.

(B) The extra density, shown in red, illustrates the potential linker between the DUF283 and Platform domains in the 3D map of the hDicer-TRBP complex.

(C) Secondary structure prediction of the linker region.

(D) EM density map with each domain colored as in the schematic illustration of Figure 1A in a view orthogonal to (B). The potential location of the unknown domain, located between the Connector and RNase IIIa domains, is marked by a gray sphere. The corresponding density is marked by the red arrowhead in the 2D class average shown in the inset.

(E) Secondary structure prediction of the unknown domain.

(F) The insertion that lacks atomic models within the RNase IIIa domain from residues 1378 to 1552 is marked by the dashed oval.

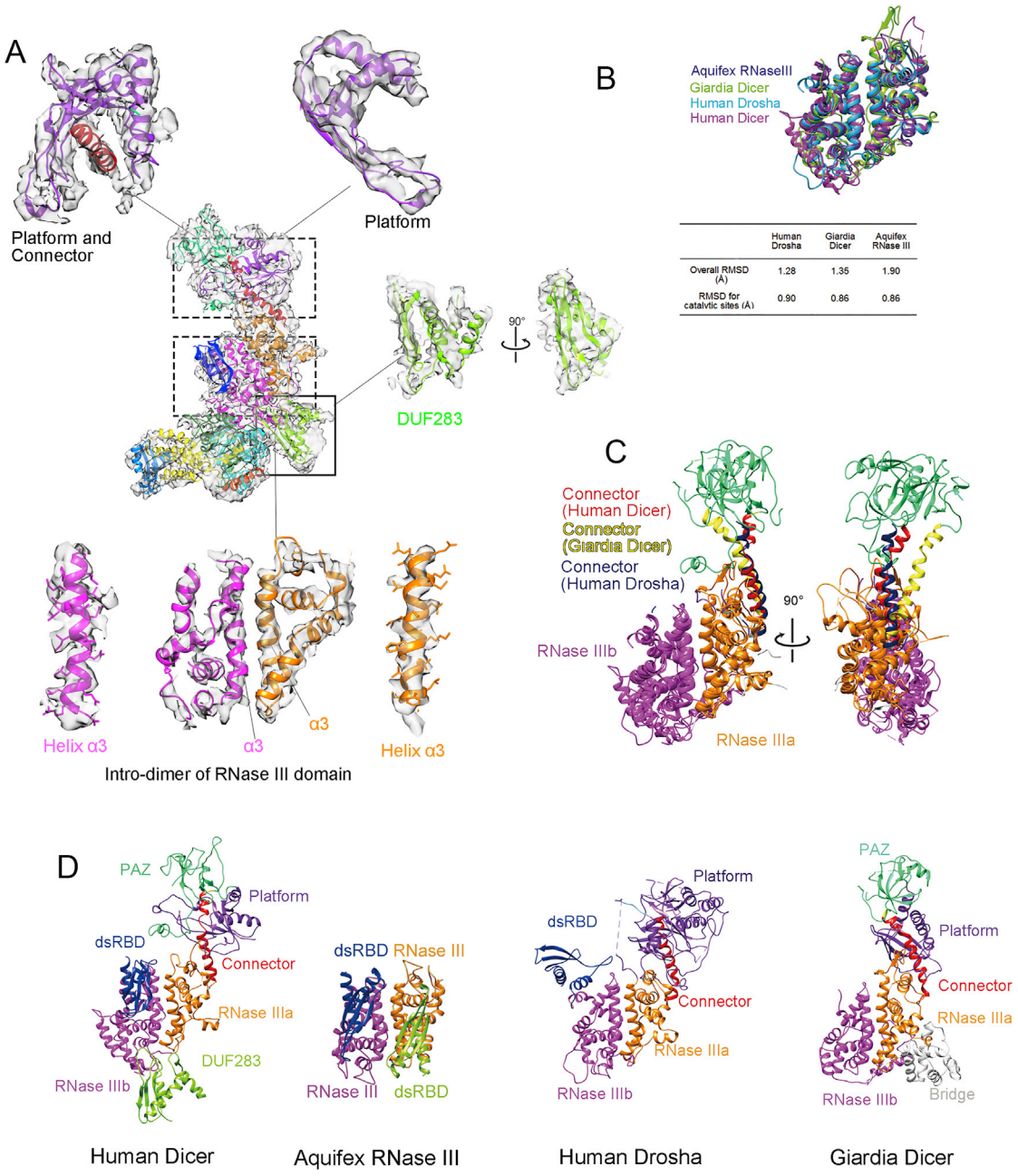

Figure S4. Comparison of Different RNase III Family Proteins, Related to Figures 1 and 4

(A) Fitting of the atomic models in different regions of the hDicer-TRBP complex 3D map, with the EM density shown in semi-transparence. The color code for the atomic models of different domains is the same as in Figure 1.

(B) Superposition of the processing-center atomic models of typical RNase III members: Aquifex RNase III is colored in purple (PDB: 2EZ6), Giardia Dicer in green (PDB: 2FFL), human Drosha in cyan (PDB: 5B16), and human Dicer in magenta. The RMSD between hDicer and its homologs are listed.

(C) Atomic models of hDicer, hDrosha and Giardia Dicer with their processing center aligned and superimposed. The PAZ domains and Connector motifs are respectively labeled in the same color for different proteins.

(D) Structures of RNase III processing centers with their surrounding domains: hDicer with the DExD/H-box helicase domain removed; Aquifex RNase III (PDB: 2EZ6); hDrosha (PDB: 5B16); Giardia Dicer (PDB: 2FFL).

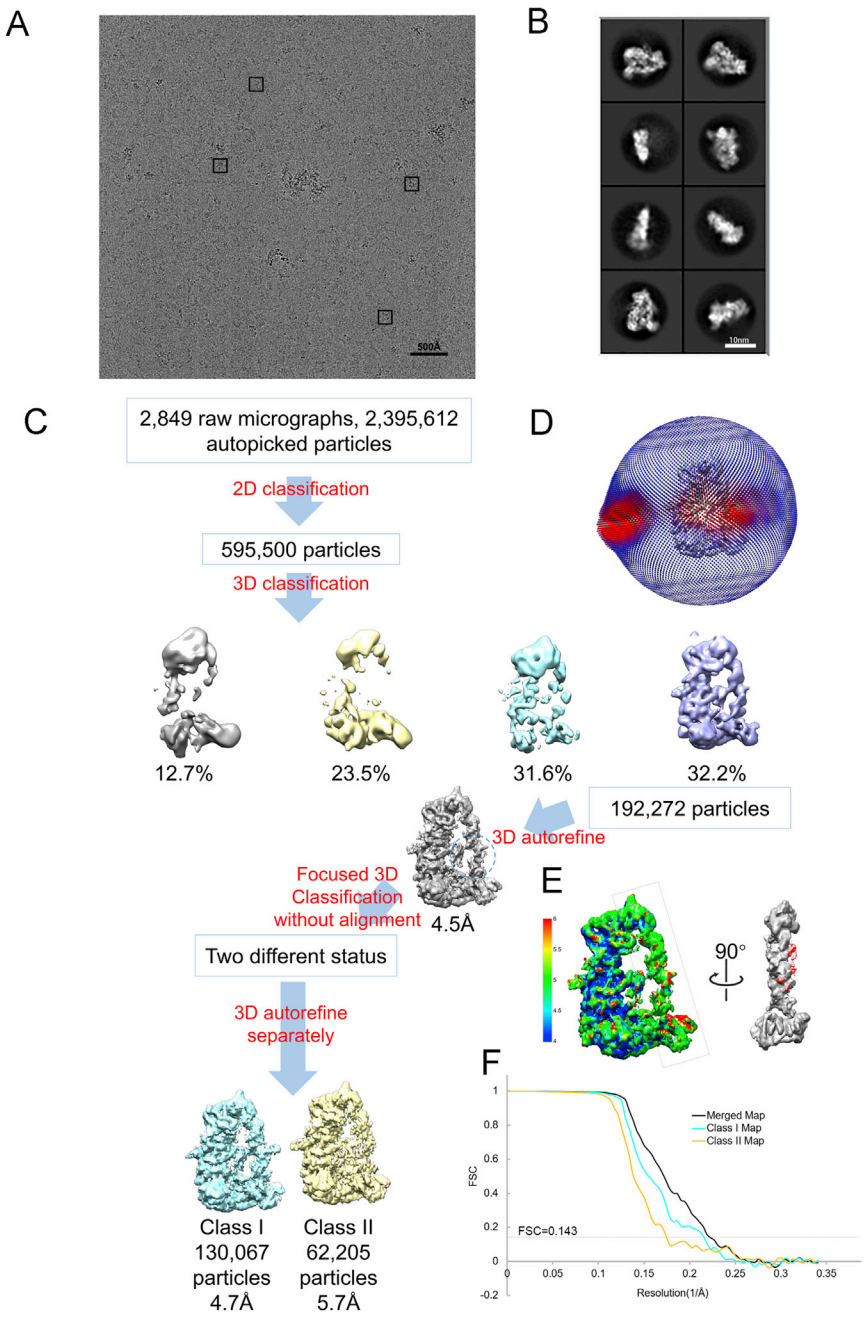

Figure S5. Cryo-EM Reconstruction of the hDicer-TRBP-Pre-let-7 Complex, Related to Figures 2, 3, and 5

(A) A representative area from a micrograph of the hDicer-TRBP-pre-let-7 complex in vitreous ice. Typical particles are marked in black boxes.

(B) Typical 2D class averages of the complex.

(C) Schematic outline of the image processing steps of hDicer-TRBP-pre-let-7 complex. Classification of the 4.5 Å resolution reconstruction that mainly focused on the pre-let-7 loop region yielded two different reconstructions at 4.7 Å and 5.7 Å resolution, respectively.

(D) Angular distribution of particles for the final 3D reconstruction.

(E) Local resolution map of the 4.5 Å resolution reconstruction estimated using RESMAP. Extra densities surrounding pre-let-7 are colored in red, potentially representing the first two dsRBDs of TRBP.

(F) Corrected FSC curves of the 3D reconstructions in RELION. Merged map: black; class I map: cyan; class II map: yellow.

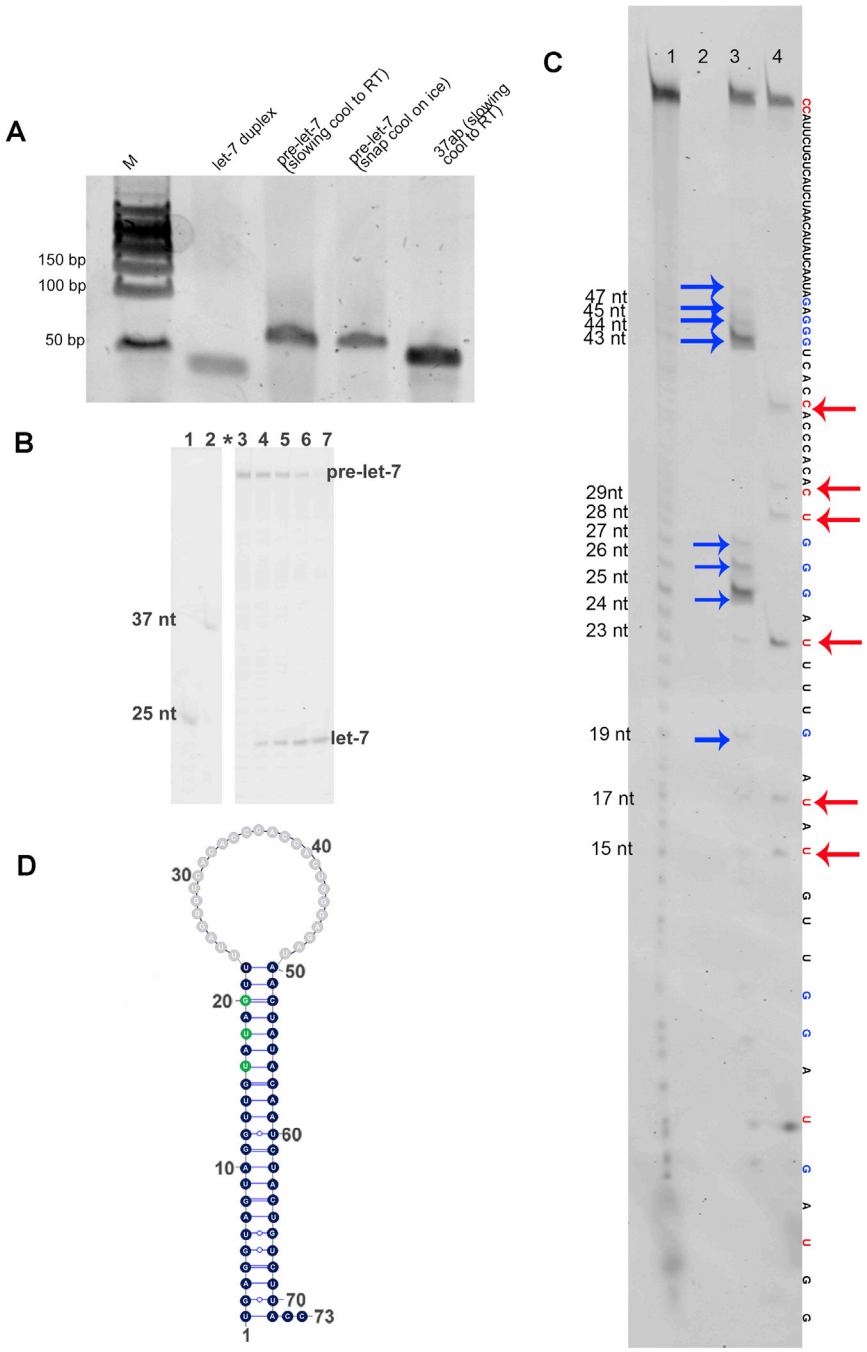

Figure S6. Biochemical Characterization of Pre-let-7, Related to Figure 3

(A) Refolded pre-let-7 under different conditions were resolved on native gel.

(B) After hDicer-TRBP-pre-let-7 complex was assembled on ice, 2 mM Mg^{+} was added into the reaction and then incubated at 37°C with a time course. The reaction products were analyzed with urea sequencing PAGE gel. Lane 1 is a 25 nt marker and lane 2 is a 37 nt marker. * indicates the irrelevant lanes removed. Lane 3-7 are the reaction products of hDicer-TRBP-pre-let-7 complex added with Mg^{2+} and incubated for 0, 5, 10, 30, and 60 min at 37°C, respectively. The RNA pre-let-7 was labeled at its 5′ terminus with FAM.

(C) RNase limited digestion of pre-let-7 analyzed on urea sequencing PAGE gel. Lane 1 is a ladder produced by alkaline hydrolysis of pre-let-7 labeled at its 5′ terminus with FAM. Lane 2 is an empty lane. Lane 3 is the digested products of pre-let-7 by RNase T1. Lane 4 is the digested products of pre-let-7 by RNase A.

(D) Secondary structure model of pre-let-7 with its nucleotides labeled. Blue color represents the nucleotides within the stem region. The three nucleotides that can be digested by RNases T1 and A within the stem region are colored in green.

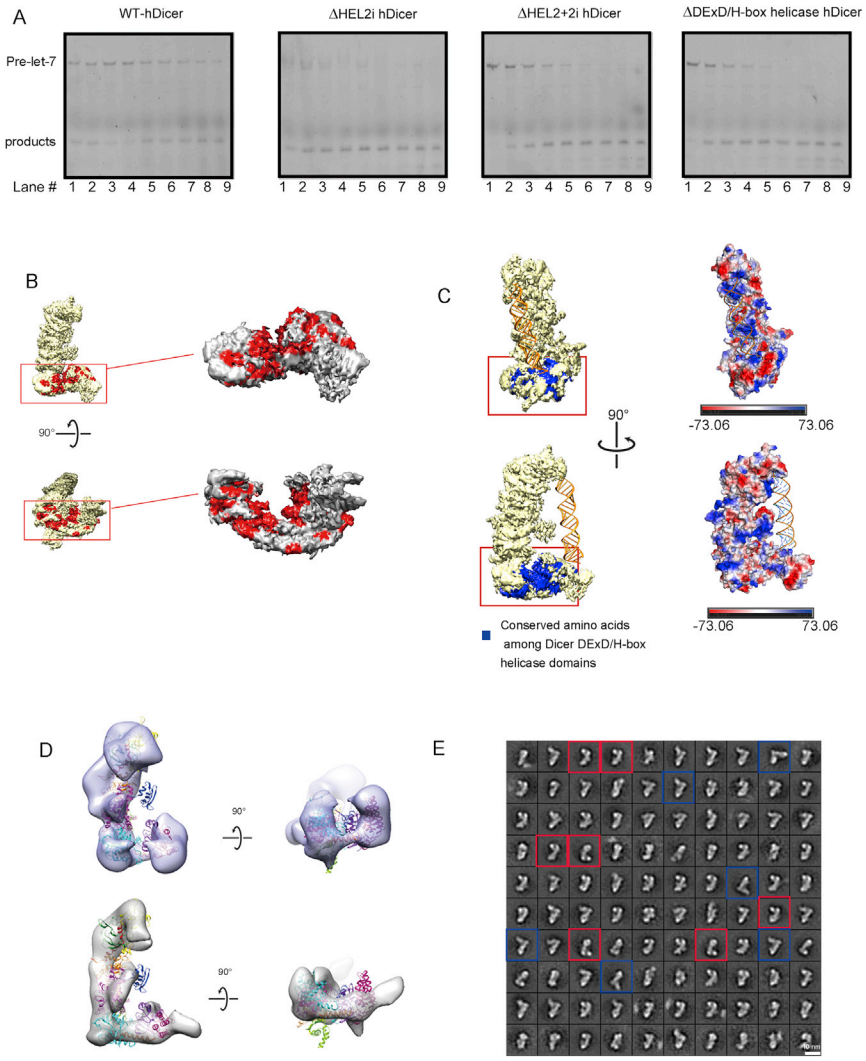

Figure S7. Analysis of the hDicer DExH/D-Box Helicase Domain, Related to Figures 5 and 6

(A) Dicing activity assay of truncation constructs with various deletion of the DExH/D-box helicase domains. Proteins was added to 100 pM pre-let-7 labeled at its 5′ terminus with FAM and the reaction was incubated with time-courses of 0, 1, 2, 5, 10, 20, 40, 80, and 120 min in lanes 1–9 respectively before running urea PAGE analysis.

(B) The most conserved amino acids among hDicer, RIG-I, and MDA5, colored in red on the hDicer-TRBP EM maps shown in two orthogonal views.

(C) The most conserved amino acids are blue-colored in the 3D EM map of the class I conformation of hDicer-TRBP complex (left panel). Electrostatic potential distribution of the whole hDicer-TRBP model (right panel). The pre-let-7 RNA is present in both panels for reference.

(D and E) Rearrangement of DExD/H-box helicase domain during the dicing reaction. A negative stained EM specimen of a dicing reaction during which the pre-let-7 was incubated with hDicer in the presence of magnesium was subjected to single-particle 3D classification. Two major classes (D) were observed to demonstrate the rearrangement of DExD/H-box helicase domain. The atomic model of the apo-hDicer was docked in both 3D volumes. (E) 2D class averages representing the two typical conformational arrangements of DExD/H-box helicase domain are marked with red and blue boxes, respectively.